Geologia Croatica
Journal of the Croatian Geological Survey and the Croatian Geological Society
2026 | 79/2 | xx–xx | 12 Figs. | 4 Tabs. | 2 Suppls. | www.geologia-croatica.hr

Tectogenic carbonate breccia (Jelar/Velebit breccia) in the Northern Velebit National Park, SW Croatia: Structural emplacement and breccia lithotypes

Bojan Matoš[1], Darko Matešić[1,*], Uroš Barudžija[1], Dubravka Kljajo[2] and Igor Vlahović[1]

[1,*] University of Zagreb, Faculty of Mining, Geology and Petroleum Engineering, Pierottijeva 6, 10 000 Zagreb, Croatia; (bojan.matos@rgn.unizg.hr; uros.barudzija@rgn.unizg.hr; igor.vlahovic@rgn.unizg.hr, *corresponding author: darko.matesic@rgn.unizg.hr)
[2] Northern Velebit National Park Public Institution, Krasno 96, HR-53274 Krasno, Croatia (geolog@np-sjeverni-velebit.hr)

doi: 10.4154/gc.2026.06
Original scientific paper

Article history:
Manuscript received: July 14, 2025
Revised manuscript accepted: February 14, 2026
Available online: May 25, 2026

Abstract

The Velebit Mt. was uplifted by multistage tectonics resulting in the formation of an approximately 150 km long, NW–SE striking anticline comprising a Late Palaeozoic to Cenozoic carbonate-clastic succession, with a major orogenic event in the younger Palaeogene. This study focused on the tectonostratigraphic investigation of a massive Tectogenic carbonate breccia (TCB) studied in the Northern Velebit area, known in the Croatian literature as the Jelar or Velebit breccia. Results of field investigations along eight profiles show that the Northern Velebit represents an ENE-verging fold formed by general E–W (ENE–WSW) contraction in the hangingwall of the NNW–SSE oriented fault, a terminal strand of the NW–SE striking Bakovac Fault Zone. The Palaeogene (–Early Miocene?) and post-Early Miocene tectonic activity resulted in NNW–SSE/ESE–WNW oriented compression, followed by NE–SW and NW–SE extension as a result of the gravitational collapse of the Northern Velebit anticline. N–S and E–W striking dextral/sinistral faults suggest NW–SE/NE–SW and ESE–WNW oriented transpression/transtension in the Northern Velebit area after the Early Miocene. Repeated structural reactivation/tectonic inversion within the Northern Velebit anticline hinge area affected the Jurassic–Cretaceous carbonates, especially along the strike of the fault/fracture systems, which resulted in prolonged brittle deformation, i.e., cataclasis, brecciation, and formation of the TCB. Within the part of the study area marked as carbonate breccia on existing geological maps, on average, 67% of eight studied profiles are actually composed of Upper Jurassic and Cretaceous limestones (and some dolomites). Between those rocks and the TCB typically a transitional zone from metres to a few tens of metres wide can be observed, composed of (1) intensely tectonised limestones/dolomites, and (2) crackle/mosaic carbonate breccia, covering approximately 12% of the total profile length. Tectogenic carbonate breccia in the study area are mostly represented by (3) monomictic carbonate breccia and (4) polymictic carbonate breccia, while (5) carbonate conglomerates and breccia-conglomerates form only rare small lenses. TCB lithotypes crop out along approximately 21% of the profile length marked as carbonate breccia on the existing geological maps of the study area. Most of the TCB outcrops were observed in the central zone of the Northern Velebit, while intensely tectonised limestones, crackle/mosaic carbonate breccia and Upper Jurassic and Cretaceous carbonate rocks predominate in the eastern and western parts.

Keywords: Velebit Mt., External Dinarides, Palaeogene (–Early Miocene?) stress regime, post- Early Miocene stress regime, fractured limestone, crackle/mosaic breccia, monomictic/polymictic carbonate breccia, Jelar/Velebit breccia

INTRODUCTION

The Velebit Mt., a large karstic geomorphostructure situated along the eastern Adriatic Sea coast, incorporates the northern part of the Dinaric orogenic belt that extends from Senjska Draga in the NW to the Zadar hinterland in the SE (Fig. 1; e.g., VLAHOVIĆ et al., 2012; ŽEBRE et al., 2021). With a length of almost 150 km and averaging 14 km in width, Velebit Mt. (the third highest mountain in Croatia, highest peak at 1757 m a.s.l.) is composed almost completely of carbonate rocks, showing extensive mechanical and chemical weathering forming variable types of karstic landforms and subsurface features often influenced by Quaternary glacial processes (SARIKAYA et al., 2020; ŽEBRE et al., 2021 and references therein). As a part of the External Dinarides, Velebit Mt. was the subject of numerous studies that extensively investigated its geomorphological properties (e.g., CVIJIĆ, 1893; ROGLIĆ, 1963; BOGNAR et al., 1991; VELIĆ et al., 2011, 2017; SARIKAYA et al., 2020; ŽEBRE et al., 2021 and references therein), as well as the tectonostratigraphic and thermochronological evolution in the frame of the Adria Microplate–Eurasian Plate collision (e.g., BAHUN, 1974; TARI KOVAČIĆ & MRINJEK, 1994; PRELOGOVIĆ et al., 1995, 2004; VLAHOVIĆ et al., 2005; SCHMID et al., 2008; KORBAR, 2009, 2025; ŚRODOŃ et al., 2018; BALLING et al., 2021a, 2023).

Though conducted studies unambiguously show all the complexity of Mesozoic–Cenozoic tectonic processes that influence polyphase formation and evolution of the Velebit Mt.,

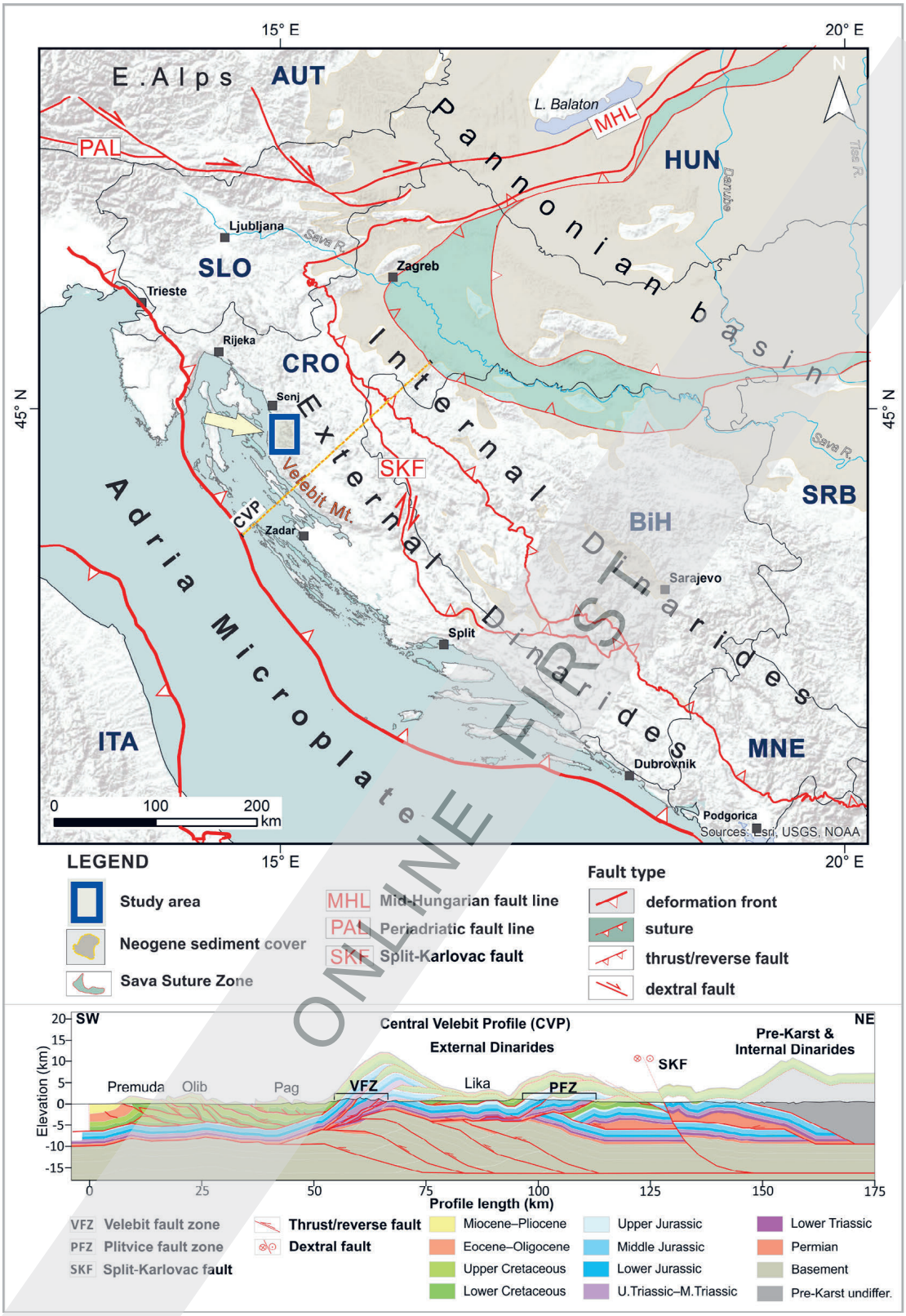

Figure 1. Tectonostratigraphic domains of the Dinarides, Eastern Alps, Pannonian Basin and Sava Suture Zone delineated by regional faults (after SCHMID et al., 2020). Central Velebit Profile (CVP) showing structural and geological architecture in the central part of the Velebit Mt. area and its hinterland (after BALLING et al., 2023). The studied area of the Northern Velebit National Park is indicated with a blue rectangle

the spatial presence of the thick and highly heterogenous Palaeozoic–Cenozoic succession (Fig. 2) combined with distinctive structural patterns, still leaves many open questions regarding the structural evolution at the local scale. This particularly refers to the specific relationships between the observed tectonic structures in the Velebit Mt. area and the extensive cover of carbonate breccia, here referred to as the Tectogenic carbonate breccia (TCB), and usually in Croatian literature referred to as the Jelar deposits (or Jelar formation, Jelar beds, Jelar breccia, Jelar group; e.g., BAHUN, 1962, 1963, 1974,

1984; SAKAČ et al., 1993a, b; TARI KOVAČIĆ & MRINJEK, 1994; KORBAR, 2009, 2025) or Velebit breccia (e.g., VLAHOVIĆ et al., 2012; BALLING et al., 2023). In this study, we focus on understanding the tectonic framework of the northern segment of Velebit Mt. belonging mostly to the Northern Velebit National Park, its structural architecture and structural control on formation of the extensive TCB and closely related intensely tectonised carbonate rocks. This research incorporated extensive structural-geological investigations that combined structural data measurements and analysis, as well as geological mapping along the predefined profiles focused on sampling and identification of different lithotypes of intensely tectonised limestones and the TCB.

Significant new research should be undertaken before attempting formalisation of this breccia as the formal litho-stratigraphic unit, so for now it could be useful to use the generic term TCB for tectonic-related breccia occurrences formed due to Palaeogene tectonics in the External Dinarides. However, we do not suggest abandoning the Jelar/Velebit breccia terms, since these terms will probably be used for the future formalisation. Besides explanation of the breccia's genetic interconnection with the orogeny of the External Dinarides, the TCB terminology is advantageous as similar massive carbonate breccia occurrences could be interpreted and named in the same manner in future studies within other Circum-Mediterranean orogens as well as in other areas.

Breccias are one of the least studied types of sedimentary rocks for several reasons, from the often very spatially limited areas of their outcrops, which makes it difficult to display them on geological maps, to the usually polygenetic and polyphase origin that results in local great variability in their properties. Also, as often being the weakest parts of the structure, they are frequently subsequently tectonised which further increases the influence of diagenesis that masks their original features. Dating breccias also represents a special challenge, since their age can often only be determined by indirect methods because they commonly do not contain index fossils in the matrix and are rarely suitable for absolute dating.

This research represents a contribution to the study of Tectogenic carbonate breccias which cover a large area of the External Dinarides – approximately 1000 km2 according to the existing geological maps of the area (Table 1).

2. TECTONO-GEOLOGICAL SETTING

2.1. Velebit Mt. tectonic evolution

The Velebit Mt. as part of the Dinaric orogenic belt formed by thin-skinned thrusting along the NE margin of the Adria Microplate which peaked during the middle to late Eocene (–early Oligocene?) (e.g., TARI KOVAČIĆ & MRINJEK, 1994; TARI, 2002; VLAHOVIĆ et al., 2005; SCHMID et al., 2008, 2020; BALLING et al., 2021b, 2023). This almost 150 km long NW–SE striking asymmetric structure is composed of intensely folded Mesozoic–Cenozoic sedimentary sequences affected by cogenetic faults showing repeated structural reactivation and inversion via several km-scale translations and rotations. Velebit Mt. tectonic evolution was discussed in several studies proposing three different evolutionary scenarios.

The first scenario proposed by BAHUN (1974), TARI KOVAČIĆ & MRINJEK (1994) and PRELOGOVIĆ et al. (1995, 2004) suggests that Eocene–Oligocene tectonic uplift of the Velebit Mt. structure occurred in a hangingwall of the presumed regional NE-dipping reverse fault, referred to as the Velebit fault, which should strike either along the Adriatic coastline or could be positioned in the immediate offshore, i.e. along the Velebit Channel.

In the second scenario, KORBAR (2009, 2025) suggested that the Velebit represents a positive flower structure formed along the presumed NE-dipping Cenozoic Velebit transpressive dextral-reverse fault. That fault as a part of the NE Adriatic fault zone should have accommodated Eocene–Oligocene compression and caused formation of the Velebit structure with its pronounced highly tectonised stratigraphic cover i.e., the Jelar carbonate breccia (or TCB herein).

The third scenario proposed by BALLING et al. (2021b, 2023), based on the mechanical stratigraphy and 2D forward kinematic modelling, suggested formation of the Velebit Mt. monocline as a hangingwall structure (see VFZ in Fig. 1) of the SW-dipping Lika passive backthrust. According to these authors, tectonic uplift of Velebit Mt. commenced during Eocene–Oligocene folding and thrusting, along the inherited and tectonically inverted Mesozoic NE-vergent backthrusts which formed a 75 km wide triangular structure (see the Central Velebit Profile in Fig. 1), that accommodated at least 44 km of horizontal shortening. The authors also proposed that such a triangle structure is built of the thin-skinned NE-vergent backthrusts composed of Palaeozoic strata detached from the SW-vergent thick-skinned antiformal stack composed of the lower Palaeozoic Adria Microplate basement (Fig. 1). Based on seismicity and structural data, BALLING et al. (2021b, 2023) suggested that the Velebit Mt. structure accommodates predominantly strike-slip motion.

It is clear that these aforementioned scenarios proposed for a tectonic evolution of the Velebit Mt. are kinematically and structurally different, but it should be noted that their accuracy and validity are based on available Mesozoic–Palaeogene outcrops, which are in large areas covered by massive outcrops of carbonate breccia (the TCB) which are in many areas masking important tectonic contacts and fault zones (VLAHOVIĆ et al., 2012).

Though it is considered that tectonic uplift and formation of the Velebit Mt., as well as the entire Dinaric orogenic belt (both Internal and External Dinarides) climaxed in the Eocene–Oligocene, available data on the present day stress field and GPS data, confirm ongoing horizontal stress field perturbations along the Dinarides due to the N- to NNE-ward directed Adria Microplate–Eurasian Plate convergence at rates between 3 and 4.5 mm/year (GRENERCZY et al., 2005; D'AGOSTINO et al., 2008; CAPORALI et al., 2009; WEBER et al., 2010; MÉTOIS et al., 2015). These convergence rates are horizontally partitioned at the scale of 1–1.5 mm/year along the East Adriatic coastline and 2 mm/year across the Dinarides, mostly accommodating thrusting and strike-slip faulting processes along the fault systems (HERAK et al., 2005; KASTELIC et al., 2013; USTASZEWSKI et al., 2014; GOVORČIN et al., 2020).

2.2. Lithological succession of the study area

The lithological succession of the External Dinarides including Velebit Mt. is characterised by predominantly shallow marine carbonate platform deposits up to 8000 m in thickness (TIŠLJAR et al., 2002; ŚRODOŃ et al., 2018). Tectonic complexity combined with palaeogeographic differences yielded lithological successions that are often highly variable both spatially and vertically (e.g., VLAHOVIĆ et al., 2005; SCHMID et al., 2020; BALLING et al., 2021b; and references from Table 1).

In the Velebit Mt. area the oldest sedimentary succession began with an approximately 2000 m thick succession of Upper Carboniferous to Lower Triassic siliciclastic rocks, dolomites and limestones (RAMOVŠ et al., 1990; ALJINOVIĆ et al., 2008; FIO et al., 2010; ISOZAKI et al., 2011). Deposited along the Gondwanian passive continental margin, these deposits were covered by Middle Triassic thick-bedded to massive limestones deposited in lagoonal environments with beds and lenses of sandstones, shales, cherts, and volcanoclastic material. Middle Triassic deposits, as the oldest rocks in the studied Northern Velebit area (Fig. 2), are 700–1400 m thick and such a difference in thickness is a result of the variable duration of the regional emergence lasting from the early or late Middle Triassic to middle Late Triassic, caused by extensional differentiation and separation of the Adria

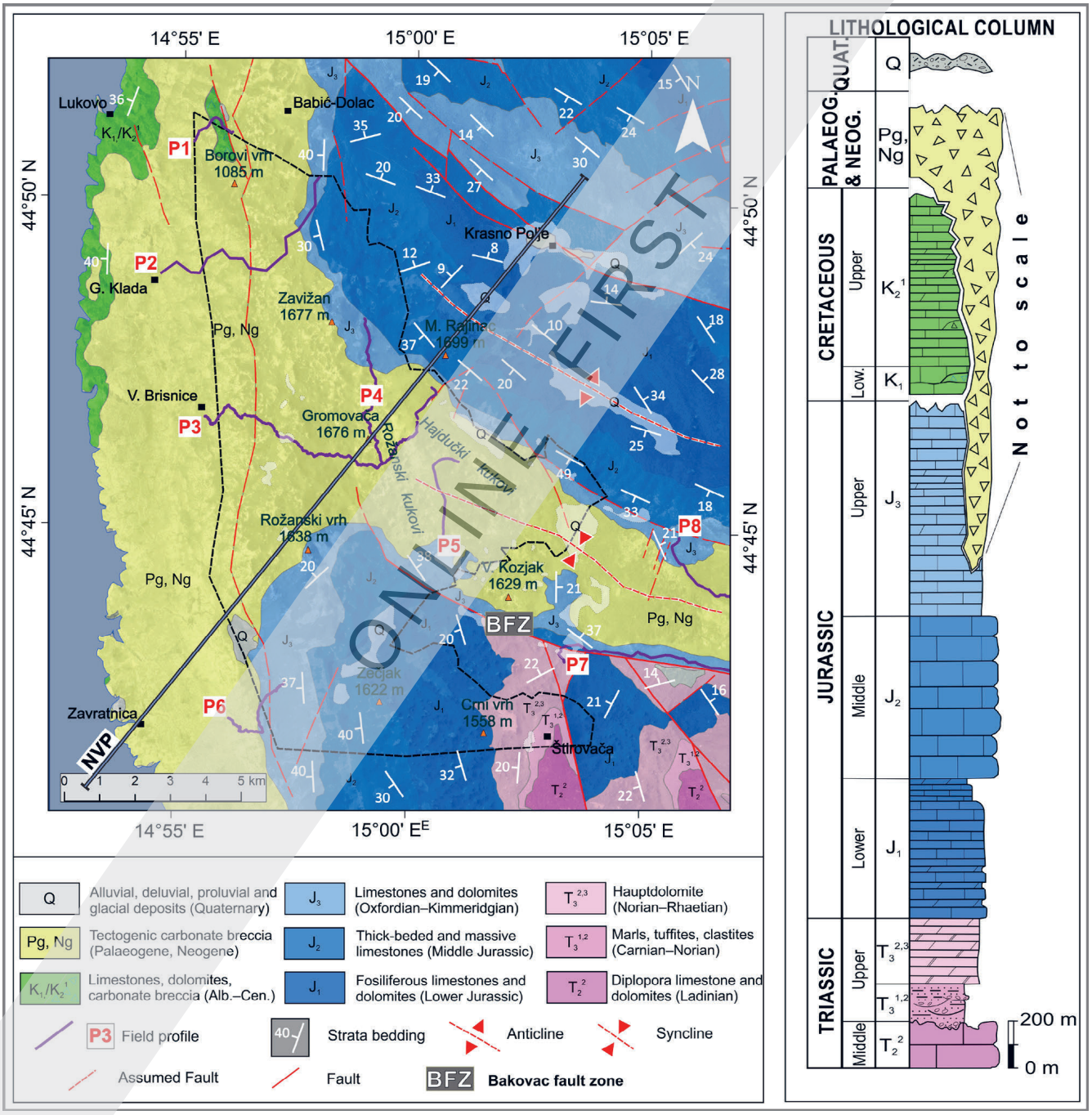

Figure 2. Geological map and lithological column of the Northern Velebit National Park and surrounding area (after MAMUŽIĆ et al., 1969; VELIĆ et al., 1974). Due to the rugged, highly dissected karstic landscape, geological and structural field investigations were focused along the existing mountain trails and pathways marked as P1 to P8 profile lines. Schematic geological profile NVP (Northern Velebit Profile) is shown in Figure 12

Microplate (MAMUŽIĆ et al., 1969; VELIĆ et al., 1974; VLAHOVIĆ et al., 2005; SMIRČIĆ et al., 2018, 2020). This tectonic segmentation enabled considerable movement of the Adria Microplate towards the north and relative isolation within the Tethyan realm, enabling stable subsidence and deposition of carbonates, several thousand metres thick, in almost ideal conditions from the Middle Triassic to the end of the Cretaceous (Fig. 2; VLAHOVIĆ et al., 2005, and references therein). During the long-lasting emergence in the Velebit area, the succession of clastic rocks known as the Raibel deposits, of highly variable thicknesses (mostly 0–100 m, rarely thicker) was deposited, and eventually covered by an approximately 400 m thick sequence of Upper Triassic dolomites (the so-called Hauptdolomit). The Lower Jurassic succession is represented by a ≈700 m thick alternation of limestones and dolomites followed by Lithiotid limestones and Fleckenkalk (spotted limestones; see Fig. 2). The Lower Jurassic carbonates are covered by a ≈2000 m thick sequence of Middle and Upper Jurassic limestones characterised by thick-bedded, massive and well-bedded limestones that often show alternation of small-scale depositional cycles.

The youngest Mesozoic rocks in the study area are Cretaceous shallow-marine carbonates that are within the Northern Velebit National Park in contact with Tectogenic carbonate breccia (TCB). With a rugged landscape, intensively karstified surface (Fig. 3) with karstic towers and numerous caves and pits, this informal lithostratigraphical unit is characterised by poorly sorted carbonate clasts that were usually tectonised before deposition, and vary in size from less than one mm to a couple of centimetres (VLAHOVIĆ et al., 2012). Composed of clasts mostly originating from the surrounding Jurassic and Cretaceous bedrock (rarely including Palaeogene clasts), such carbonate breccia deposits according to data from Basic Geological Maps cover more than 1000 km2 of the External Dinarides (Table 1) and locally exceed more than 600 m in thickness (see VLAHOVIĆ et al., 2012 for details).

The youngest Quaternary cover of the Velebit area is represented by several metre thick moraine deposits found in Northern Velebit with absolute ages between 94.0 ± 24.0 ka and 9.0 ± 0.8 ka (ŽEBRE et al., 2021).

2.3. Review of Tectogenic carbonate breccia research in the External Dinarides

Tectogenic carbonate breccia (TCB; in the Croatian literature usually referred to as Jelar or Velebit breccia) together with the youngest alluvial part of the Promina deposits (ZUPANIČ, 1969; MRINJEK, 1993; TARI KOVAČIĆ & MRINJEK, 1994), the largest areas of which occur in southeasternmost Velebit Mt. area and Northern Dalmatia south of Obrovac and Karin (Fig. 1), represent the two largest coarse-grained clastic lithostratigraphic units within the External Dinarides. Large outcrops of breccia were first studied in the early 20th century during geological mapping of the Austro-Hungarian Monarchy. On those historical maps breccia deposits were mostly referred to as Grey Lower Cretaceous breccia or Lower Cretaceous breccia and limestones on Velebit Mt. and the surrounding areas (e.g. SCHUBERT, 1908, 1909; SCHUBERT & WAAGEN, 1912), or as Rudist limestones and breccia of the Lower and Upper Cretaceous on the island of Krk and surrounding areas (e.g. WAAGEN, 1905, 1908), based on the age of the predominant clasts and limestones found between breccia outcrops. On some of the later published maps of the Velebit area, the breccia deposits were addressed as Grey breccia of Velebit (e.g. SCHUBERT, 1920a, b), while KOCH (1929) referred to them as Lower Cretaceous grey and multicoloured breccia. Very small bodies of conglomerates with some younger Upper Cretaceous and Palaeogene clasts found within breccia deposits were determined as part of the Promina deposits (SCHUBERT, 1909; SCHUBERT & WAAGEN, 1912; KOCH, 1929).

Subsequently, until the 1960's, the massive carbonate breccia occurrences were considered to be part of the so-called Promina deposits of Velebit and Lika (POLJAK, 1938; POLŠAK, 1957; CRNOLATAC & MILAN, 1959; BAHUN, 1962), although HERAK (1959) considered that massive carbonate breccias were not part of the Promina deposits but an older succession formed during the Cretaceous. The most comprehensive study of the carbonate breccias took place during work on the Basic Geological Map of the former Yugoslavia at 1:100,000 scale. Carbonate breccias were mapped on 13 map sheets (Table 1), but with different descriptions and stratigraphic assignments. Variable breccia stratigraphic assignments and descriptions at the scale of geological maps were due to the rough landscape and outcrop inaccessibility, complex spatial breccia occurrences and ambiguous stratigraphic/tectonic relationships to the surrounding units, which resulted in different opinions as to when formation of the breccias took place.

On these geological maps (Table 1), three distinct breccia outcrop types can be recognised: (i) extensive cover with thicknesses in places exceeding 400 m (e.g. in the Northern and Central Velebit area), (ii) numerous small outcrops, probably erosional remnants of a once more widespread and thicker breccia cover (Lika region), and (iii) elongated breccia outcrops on the Kvarner Islands (e.g. islands of Krk and Rab), mostly located within the hinge zones of large anticlines. Small carbonate breccia outcrops have also been identified in the Hrvatsko primorje (POLŠAK, 1957) and in parts of Dalmatia and Herzegovina (SAKAČ et al., 1993a, b). The largest outcrop of TCB in Croatia, covering an area of c. 690 km², extends continuously from the western and southwestern slopes of Velebit Mt., along the Bakovac Fault Zone (Fig. 2), and from the NW (Kosinj area) to the Lika region SE of Gospić. This extensive breccia outcrop accounts for more than two-thirds of the total breccia surface exposure area.

A very significant sedimentological and structural contribution was made by BAHUN (1962), who used data from a borehole near Lake Kruščica in Lika and determined that the carbonate breccias at that location were interbedded, both laterally and vertically, with brown limestones containing foraminifera and ostracods. Similar relationships were noted by IVANOVIĆ et al. (1965), although they did not mention any fossil content. Subsequently, BAHUN (1963) stressed a distinction between breccia-dominated deposits and typical Promina Beds due to significant lithological, depositional and

Table 1. Sheets of the Basic Geological Maps of SFRY at 1:100,000 scale with the associated stratigraphic age of the breccia, number of breccia outcrops and total area covered by breccia within the External Dinarides.

Basic Geological Map sheet	Authors of basic geological maps and explanatory notes	Breccia stratigraphic symbol	Number of outcrops	Area (km^2)
BIHAĆ	POLŠAK et al., 1976, 1978	E, Ol	10	1.63
CRIKVENICA	ŠUŠNJAR et al., 1970 GRIMANI et al., 1973	E_3, Ol_1	104	14.55
DRNIŠ	IVANOVIĆ et al., 1977, 1978	$^2E_2$	3	2.05
GOSPIĆ	SOKAČ et al., 1974, 1976a	E, Ol	34	273.27
KNIN	GRIMANI et al., 1972, 1975	E, Ol	1	0.76
OBROVAC	IVANOVIĆ et al., 1973, 1976	Pg, Ng	16	143.17
OGULIN	VELIĆ & SOKAČ, 1981 VELIĆ et al., 1982	E, Ol	7	5.65
OMIŠ	MARINČIĆ et al., 1976, 1977	Ol	13	21.36
OTOČAC	VELIĆ et al., 1974 SOKAČ et al., 1976b	E, Ol	71	290.14
RAB	MAMUŽIĆ et al., 1969 MAMUŽIĆ & MILAN, 1973	Pg, Ng	34	148.18
SILBA	MAMUŽIĆ et al., 1970 MAMUŽIĆ & SOKAČ, 1973	$Pg_{2,3}$	9	33.01
UDBINA	ŠUŠNJAR et al., 1973 SOKAČ et al., 1976c	Pg, Ng	103	45.58
ZADAR	MAJCEN et al., 1970 MAJCEN & KOROLIJA, 1973	$Pg_{2,3}$	1	27.70
		TOTAL	406	1,007.05

structural differences, proposing for them a new term, Jelar deposits, to be used until further, more precise stratigraphic determination was available. Originally the author estimated that these deposits comprise approximately 70% limestone breccias composed of Jurassic, Cretaceous and Palaeogene clasts, 25% massive or bedded limestones, and 5% marls and marly breccia.

BAHUN (1962, 1974) related the formation of breccias to the tectogenesis of Velebit Mt. and proposed that it occurred in two tectonic phases – a compressional phase resulting in Late Cretaceous–Palaeogene tectonic uplift of Velebit Mt., and its Palaeogene–Neogene post-uplift relaxation phase. A similar tectonic evolution was described by the same author (BAHUN, 1985) for the breccia outcrops in the Srebrenica River valley in SE Lika region, where he reclassified breccias previously considered as Upper Jurassic in age as the Jelar deposits. HERAK & BAHUN (1979) referred to these brecccias as the Jelar formation and interpreted them as a "Tertiary wildflysch" formed by "orogenic disturbances and erosion", mostly during the Palaeogene.

BAHUN (1984) identified contacts between the Jelar formation and surrounding rocks as gradual, including transitional zones from massive, undeformed limestones to increasingly fractured limestones, which within fracture zones contain angular fragments and low cement content. The same author stated that with progressive brittle deformations of already fractured limestones, the Jelar formation experienced a progressive increase in cement content and clast size variability, which gradually transitioned into a heterogeneous polymict breccia.

TARI KOVAČIĆ & MRINJEK (1994) proposed two levels of Jelar breccia based on the tectonic phases and their timing. The authors considered that Early Jelar breccia are coeval with the middle Eocene part of the flysch formation forming the base of the neighbouring Promina deposits, while the Late Jelar breccia were according to them formed during middle to late Eocene. TARI KOVAČIĆ & MRINJEK (1994) also noted that conglomerates from the youngest part of the Promina beds contain cannibalised clasts of the Early Jelar breccia (not illustrated in their paper), indicating that the youngest part of the Promina beds should be younger than the Jelar breccia. As the studied breccia deposits are generally missing stratigraphic cover, except for Quaternary deposits, findings of freshwater Pliocene marls above breccias in boreholes near Gornji Kosinj and the Zrmanja River by FRITZ & PAVIČIĆ (1975) and FRITZ et al. (1978) suggested that breccia was deposited in that area between the middle Eocene and the Pliocene.

More recent studies of the structural emplacement and breccia formation were presented by VLAHOVIĆ et al. (2012, 2018), based on their preliminary results (VLAHOVIĆ et al., 2007, 2011). The authors described breccias as massive, unsorted, clast-supported deposits, lacking visible sedimentary internal fabrics and structures. The majority of the clasts are tectonised, indicating intense tectonic activity prior to their deposition, while occurrences of cannibalised breccia clasts within the breccia suggested their polyphase evolution. The authors recognised the gradual contact with the surrounding rocks as one of the main criteria differentiating the investigated breccia from other types of breccia. The authors also noted that breccia contacts with the surrounding rocks are mostly steeply inclined to vertical and that all breccia outcrops have a common denominator: (i) Palaeogene tectogenesis (possibly even partly Neogene in age), (ii) a typical habitus almost entirely composed of carbonate clasts of the same or various ages infilled with a mostly finely crushed carbonate matrix,

and (iii) outcrops are located exclusively along the NE-verging tectonic structures, which are rare in the External Dinarides.

The same authors noted that breccia thickness in the central parts of the Velebit Mt. locally reaches more than 600 m. Based on extensive field studies, the authors suggested that massive carbonate breccias are tectonically emplaced within zones related to NE-verging overturned folds and faults, which are opposite to the almost exclusively SW-verging Dinaridic structures. VLAHOVIĆ et al. (2012) proposed a new term for these massive carbonate breccia occurrences; the Velebit breccia, as the largest and most visible breccia outcrops can be observed on Velebit Mt. and the area around it (as previously referred to more than hundred years ago as the Grey Breccia of Velebit by SCHUBERT, 1920a, b). This term was proposed to replace the original term Jelar deposits (and other derived terms, including the Jelar formation, Jelar beds or Jelar breccia), which beside breccia in the original description also included limestones and marls, especially since the type locality cannot be found on most topographic maps and a large part of the Jelar hill area near Kosinj is composed of tectonised limestones rather than carbonate breccia.

KORBAR (2009) interpreted carbonate breccias as the gravitational infill of deep, narrow extensional troughs formed within the regional Velebit Mt. anticline hinge zone, that were contemporaneously filled during extension with breccia deposits that originated from collapsed successions above the inferred detachments.

LACKOVIĆ (1993), STROJ (2004) and STROJ & VELIĆ (2015) explored breccia occurrences within deep speleological objects (Lukina jama–Trojama and Velebita cave systems), mapping breccias down to depths between 400 to 980 metres beneath the surface.

The recent study of massive carbonate breccia occurrences in the External Dinarides was presented by MATEŠIĆ et al. (2023), documenting that on the island of Krk, breccia deposits were partly accumulated in fresh-water environments, with indications of local fluvial transport. BALLING et al. (2023) differentiated occurrences of two carbonate breccia belts within the Velebit area as a result of breccia structural position: i) the mostly polymictic carbonate breccia belt (they referred to it as the Velebit breccia after VLAHOVIĆ et al., 2012), that unconformably overlies Jurassic–Cretaceous bedrock on the SW slopes of Velebit Mt., and ii) monomictic breccia (referred to as the Jelar breccia) occurring along the NE Velebit Mt. margin and Lika Plateau which overlie Cretaceous carbonates at the surface. However, KORBAR (2025) commented that both types of breccia are probably of the same genesis, as well as those along the Dabarski kukovi, and that they all differ from breccia cropping out in eastern Lika (upper stream of Una River, BAHUN, 1985).

BALLING et al. (2023) also interpreted occurrences of carbonate breccias along the Dabarski kukovi in Central Velebit Mt. as fault monomictic cataclastic breccias, composed of reworked Upper Jurassic clasts, formed exclusively within the footwall of the regional Brušane–Oštarije fault. However, our studies in the area documented that besides the cataclastic breccia predominantly composed of Upper Jurassic clasts, derived from the neighbouring limestones, along the Dabarski kukovi there are also common findings of polymictic breccias with sporadic conglomerate lenses, comprising Upper Cretaceous and Palaeogene clasts, which is clear evidence that the majority of the breccia actually represent the TCB described here, and only further documents their complexity.

Our recent investigation of the TCB in different areas of the Hrvatsko primorje including the Kvarner islands, Velebit Mt. and Lika, helped us to recognise specific structural and petrological properties which further complement the detailed breccia description provided by VLAHOVIĆ et al. (2012) for breccias on the Velebit Mt. That said, within the studied breccias and genetically related tectonised limestones (less often dolomites), there is a significant diversity in grain composition, the quantity and characteristics of the matrix, sporadic presence of lenses of fine-grained deposits, sandstones or conglomerates. They may be found in different structural positions, and with specific contacts with neighbouring carbonate units (e.g., usually inclined to vertical gradational contact with transitional zones between homogenous carbonates and the TCB, in places tectonic contacts).

3. MATERIALS AND METHODS

3.1. Structural mapping and data analysis

This study of the structural relationships and Tectogenic carbonate breccia properties in the Northern Velebit area was carried out from 2019 to 2023 as part of the scientific research funded by the Public Institution Northern Velebit National Park. Extensive geological and structural investigations resulted in data collection from 533 field locations (Fig. 3; S1), along the eight geological profiles (58.7 km length in total; Fig. 2). Geological and structural data were georeferenced using ESRI ArcMap GIS software; the field data collection included detailed lithological descriptions, measurements of the bedrock planar/linear geometric properties, as well as bedding and associated fracture system measurements. The database also included measurements of outcrop-scale fault geometric properties and kinematic indicators, which were of special interest due to their importance in understanding structural relationships between mapped units and their kinematic history.

The collected dataset of bedding, foliation, fracture systems and faults comprised 137, 53, 397 and 68 measurements, respectively. At the local scale, visible fold axes orientations were determined. Collected structural data of bedding, foliation and fracture system orientations were analysed with the Stereonet v.11 software (ALLMENDINGER et al., 2011; CARDOZO & ALLMENDINGER, 2013).

For measured bedding, foliation and fracture systems data, average orientation planes were calculated graphically, using the most common data orientation, within a 10% area coverage domain. Fracture system analysis incorporated contour plot constructions of the fracture pole distribution, using the 1% area contour method (ALLMENDINGER et al., 2011; CARDOZO & ALLMENDINGER, 2013). Contour plot distribution, i.e. frequency distribution, was used to determine representative fracture sets in the studied domains.

Determination of fault kinematics was based on the geometric properties data (i.e. dip direction, dip angle) of fault

planes and their kinematic indicators, i.e. slickenside orientations defined by azimuth direction and plunge, and the sense of movement (DOBLAS, 1998). As a result, based on the kinematic criteria, measured faults and shear planes were analysed and processed by TectonicsFP v. 1.7.9 software (ORTNER et al., 2002), with their separation into kinematically compatible fault groups. Using the P–T axis method, theoretical maximum (σ1), mean (σ2) and minimum stress axes (σ3) were further calculated (TURNER, 1953; MARRETT & ALLMENDINGER, 1990), while the synthetic focal mechanisms were calculated using the Right Dihedra Method available within the TectonicsFP v. 1.7.9 software (ANGELIER & MECHLER, 1977).

3.2. Geological mapping and sampling along the profiles

Geological mapping and breccia sampling within the Northern Velebit National Park and surrounding area was mainly performed along the existing mountain trails and pathways, due to extremely rugged and highly dissected karstic terrains that prevail in the mountainous area. Study included mapping along the eight geological profiles with a total length of 58.7 km (Fig. 2; Table 4).

Beside the structural measurements, detailed geological mapping along profiles incorporated i) identification of normal and tectonic boundaries between the different units along the profiles, and ii) study of lithostratigraphic units spatial extent along the profiles, with a special interest in the distribution of Tectogenic carbonate breccia (TCB; in Croatian literature usually referred to as Jelar/Velebit breccia), and iii) recognition of different lithotypes within the tectonised limestones and the TCB (Fig. 4).

Among the collected rock samples, 53 were cut into thin slabs (Fig. 3; for detailed locations see Suppl. S2). Prior to the preparation of microscopic slides, the slab surfaces were polished and documented using scanner or/and SONY α7 IV camera equipped with a LAOWA 100 mm Ultra Macro lens, offering a maximum magnification ratio of 2x. For micropetrographic observations, standard petrographic thin-sections of 30 μm thickness were prepared, some of which were stained with Alizarin Red S to distinguish between calcite and dolomite components.

The petrographic descriptions of thin-sections were based on the proportion and relationship between the cement, matrix and clasts, the diversity in composition, age and size of the clasts, their arrangement and sorting, the shape of the clasts (roundness/sphericity), the type of material between clasts (matrix/cement) and its characteristics, as well as the presence and distribution of fractures and pressure-dissolution features (stylolites/dissolution seams).

Based on field observations and detailed sample analyses, classification of tectonised and brecciated rocks in the study area included the following lithotypes: i) intensely fractured limestones, ii) crackle/mosaic carbonate breccias (cf. MORT & WOODCOCK, 2008; WOODCOCK & MORT, 2008; FLUDE et al., 2025), iii) monomictic carbonate breccias, iv) polymictic carbonate breccias (matrix-supported or clast-supported), and v) carbonate conglomerates and breccia-conglomerates.

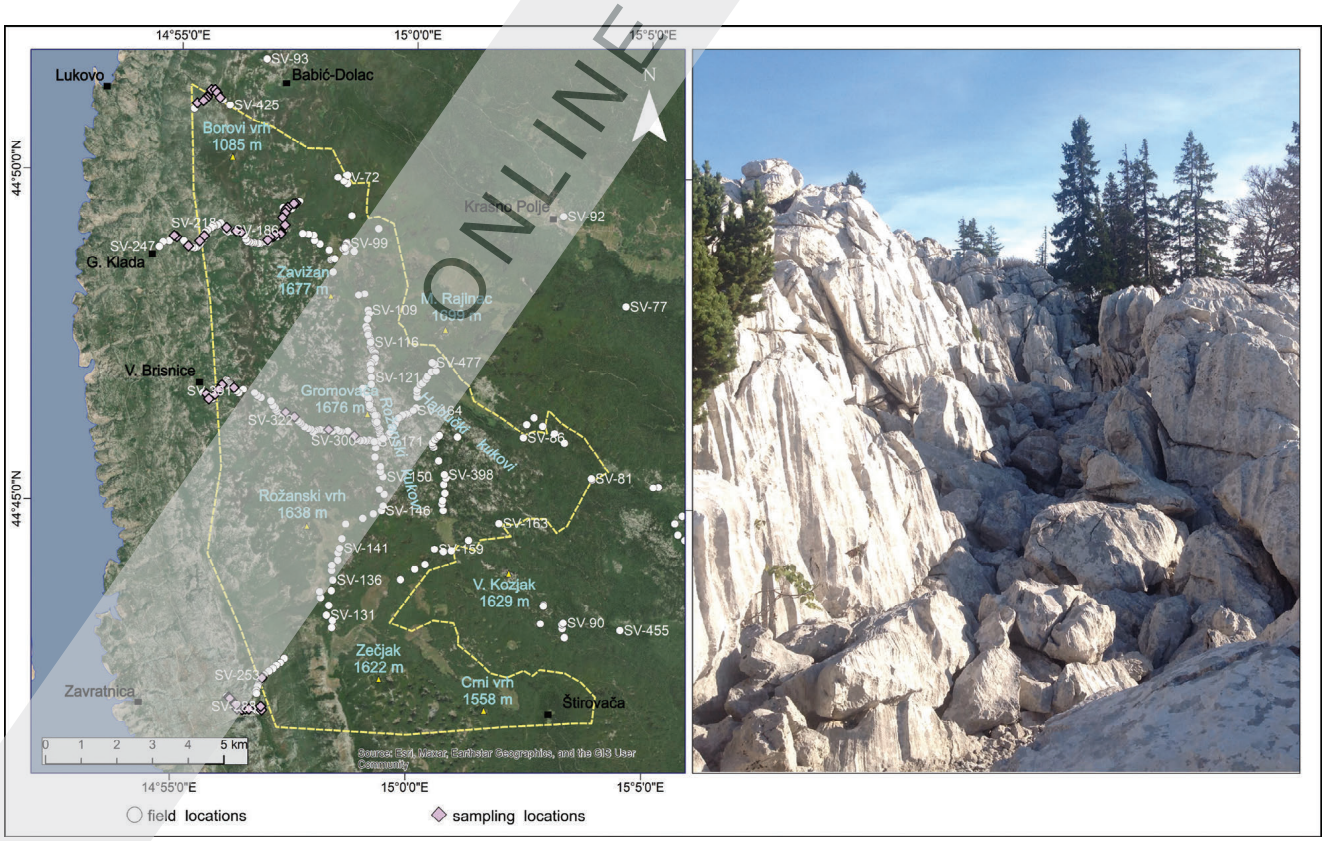

Figure 3. Map of the study area with field locations and sampling site locations on the left. For sampling site location coordinates see S2. Geological mapping, rock sampling and structural measurements were performed along eight geological profiles, at 533 field locations. The yellow polygon outlines the Northern Velebit National Park area. The figure to the right shows representative intensively karstified landscape of breccia within the central part of the National Park area (slope of Gromovača peak – 1676 m), along the Premužić hiking trail (Field location SV-117; 44.787°N, 14.987°E)

4. RESULTS

4.1. Analysis of measured bedding, foliation and fracture systems

Structural measurements within the Northern Velebit National Park were mostly conducted within the area covered by Tectogenic carbonate breccia (TCB in approximately 360 field locations), while measurements within the Mesozoic carbonate complex were conducted in approx. 170 field locations. Beside the characteristic karstic landforms (e.g., sinkholes, dolines, karrens, grikes, poljas, valleys, caves, etc.), the studied terrain is very dissected, being characterised by systematic fracture systems that caused formation and selective erosion of the bedrock.

A total of 137 measured strata (bedding planes) within Mesozoic carbonates indicate folded structures dipping mostly towards the E and W, with an average dip angle between 23° and 44° (see Table 2; Figs. 4, 5). Measured bedding orientations indicate gentle folds (interlimb angles between 100 and 130°), characterised by subhorizontal fold axes trending predominantly N–S, locally NNW–SSE (see Table 2; Fig. 5). The prevalence of N–S (locally NNW–SSE) trending fold axis orientations suggests a relatively uniform long-term stress field within the study area which enabled fold formation and preservation, without evidence of possible rotation or translation caused by a secondary tectonic overprint.

The measured fracture data set composed of 397 measurements suggests the existence of six main fracture systems in the studied area (Table 2; Fig. 5). All fracture systems are characterised by a general N–S strike deviating either towards the NE or NW. The dominant Fs1 discontinuities (58 data) are characterised by subvertical orientation, with fractures striking N–S (Figs. 4, 5). Fracture systems Fs2 and Fs5 as well as Fs3 and Fs4 behave as conjugate fracture pairs. Fs2 and Fs5 (22 data points) combine NNE–SSW striking discontinuities dipping either towards the WNW or the ESE at an average dip angle of 48° and 61° respectively (see Table 2; Fig. 5). Fracture systems Fs3 and Fs4 (33 data) however, combine N(NNW)–S(SSE) striking discontinuities dipping either towards the W or the ENE at an average dip angle of 35° and 66° respectively (see Table 2; Figs. 5, 6a). Similar to the Fs1, fracture system Fs6 (41 data) shows subvertical geometry, characterised by a NE–SW strike (see Table 2; Fig. 5). All the identified fracture systems, characterised by a generally N–S strike, subvertical geometry and conjugate relationships, imply their structural

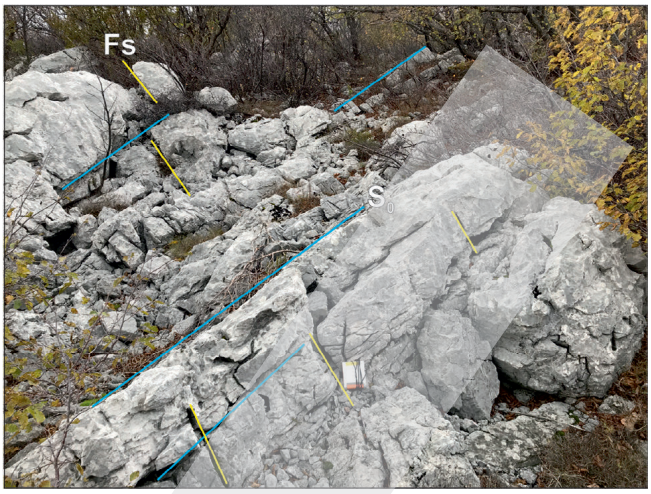

Figure 4. Upper Jurassic fossiliferous limestone cropping out along the P6 profile (for position see Fig. 2) within the southwestern section of the Northern Velebit National Park (Field location SV-249; 44.710°N, 14.955°E) with bedding orientation of 278/45 (dip direction/dip angle) deformed by N–S striking subvertical fracture system

Table 2. Average orientations of the measured bedding, foliation and fracture systems in the Northern Velebit National Park and surrounding area, and number of data in each set.

Strata bedding	Data	Dip direction (°)	Dip angle (°)	Strike
$S0_1$	22	268	44	178–358
$S0_2$	20	275	27	5–185
$S0_3$	15	94	23	4–184
$S0_4$	10	73	35	163–343
Foliation	**Data**	**Dip direction (°)**	**Dip angle (°)**	**Strike**
S_1	9	172	47	82–262
S_2	5	325	26	55–235
S_3	8	321	16	51–231
S_4	7	96	33	6–186
Fracture system	**Data**	**Dip direction (°)**	**Dip angle (°)**	**Strike**
Fs_1	58	–	–	0–180
Fs_2	13	283	48	13–193
Fs_3	6	276	35	6–186
Fs_4	27	72	66	162–342
Fs_5	9	100	61	10–190
Fs_6	41	–	–	36–216

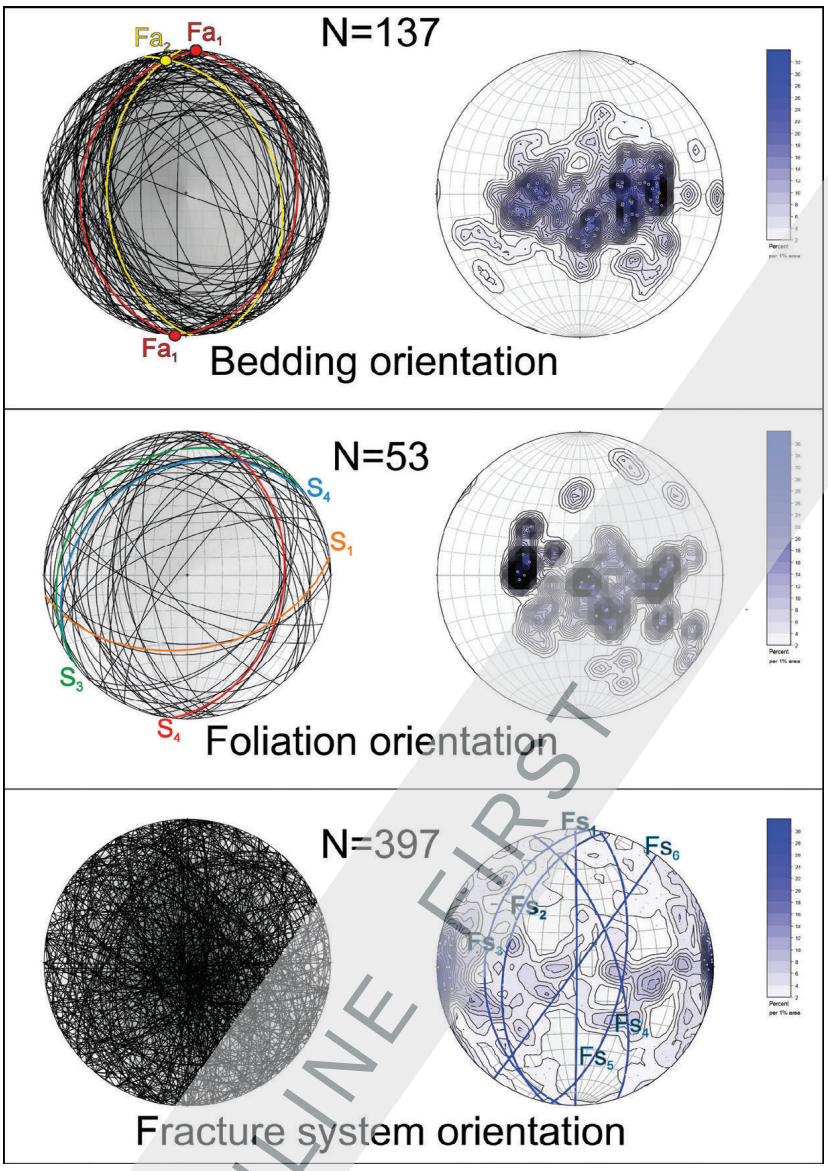

Figure 5. Bedding orientation with average fold axis, measured foliations and delineated fracture systems with average orientation within the studied part of the Northern Velebit National Park and surrounding area. Illustrated with Stereonet software, stereographic projection on the lower hemisphaere

Figure 6. **(a)** Upper Cretaceous(?) brownish micritic limestone cropping out along the P3 profile (Fig. 2) within the western part of the Northern Velebit National Park (Field location SV-289; 44.776°N, 14.928°E) with bedding orientation of 104/25 (dip direction/dip angle) and NNW–SSE striking subvertical fracture system (10/60); **(b)** Brownish micrite limestone (Upper Cretaceous(?)) along the P3 profile at the Field location SV-296; 44.766°N, 14.986°E)

Table 3. Mean geometric properties of the fault planes observed in the Northern Velebit National Park and surrounding area with calculated kinematic indicators and parameters. Fault planes were grouped on the basis of their geometric and kinematic properties (Fig. 9). Fault types: RF – reverse faults; NF – normal faults; SSF – strike-slip faults. Orientations of the P- and T-axes are based on constructed synthetic structural beach-ball diagrams.

Group	Subset	Data	Dip direction (°)	Dip angle (°)	Pitch (°)	Strike (°)	Striation		P-axis		T-axis	
							Trend (°)	Plunge (°)	Trend (°)	Plunge (°)	Trend (°)	Plunge (°)
RF1	RF1/a	4	12	62	73	–	322	52	348	9	234	68
	RF1/b	3	148	40	74	–	194	30				
RF2	RF2/a	5	264	58	59	–	298	53	278	9	39	74
	RF2/b	2	112	36	46	–	80	32				
NF1	NF1/a	13	32	60	70	–	83	48	159	61	53	9
	NF1/b	6	260	44	46	–	210	32				
NF2	NF2/a	5	320	56	68	–	350	50	130	67	331	22
	NF2/b	2	164	40	63	–	140	38				
SSF1	SSF1/a	9	202	86	6		292	0	337	2	67	2
	SSF1/b	5	–	–	11	22-202	22	2				
SSF2	SSF2/a	5	82	80	14	–	352	0	217	6	308	5
	SSF2/b	3	–	–	3	82-262	262	10				
SSF3	SSF3/a	4	322	82	9	–	236	18	282	3	192	12
	SSF3/b	2	54	74	12	–	144	10				

position within either the hinge zone or fold limbs of the existing folded structures.

Fifty-three measured foliations (Table 3; Fig. 5) resulted in determination of the ambiguous differentiation and structural relationships between bedding, fracture systems and the presence of fault planes. Measured discontinuities are grouped into S1 to S4 subsets according to their geometry. While the N–S striking foliation S4 subset dipping towards the E with an average dip angle of 33° (Table 2; Fig. 5) may correlate with strata bedding or Fs5 fracture system, the NE–SW striking foliation S1–S3 subsets dipping towards both the NW and SE (Table 2; Fig. 5) may correspond to the orientation of the observed fault groups (Table 2; Fig. 7).

4.2. Fault and palaeostress field analysis

Structural measurements of fault planes were focused on identifying fault zones dominating the area of the Northern Velebit National Park and the surrounding area comprising breccia outcrops. A total of 68 fault plane/shear fracture data were collected (Table 3; Fig. 7). Based on fault/shear fracture kinematics, geometry and stress field, the measured data were organised into three principal fault categories, subdivided into fault groups and subsets (Table 3; Fig. 7).

4.2.1. Reverse faults

Reverse fault planes (a total of 14 measurements) were separated into RF1 and RF2 fault groups (Table 3; Figs. 7, 8). The RF1 group is characterised by two fault subsets: RF1/a subset with a general NNE dip direction and average dip angle of 62° (Table 3; Fig. 4) and the RF1/b subset that dips towards the SE at an average dip angle of 40° (Table 3; Fig. 7). The second reverse fault group RF2 is composed of subsets striking generally N–S (Fig. 8), with local deviations towards the NNW and NNE. The RF2/a subset dips towards the W, with an average dip angle of 58°, while its conjugate pair the RF2/b subset is composed of planes dipping towards the ESE with an average dip angle of 36° (Table 3; Fig. 7).

Results of the palaeostress field analysis suggest that the RF1 fault group is associated with a compressional stress field and NNW–SSE trending P-axis (Table 3; Fig. 5), while the RF2 fault group, also formed in a compressional stress field, was associated with an ESE–WNW trending P-axis (Table 3; Fig. 7). These results, i.e. both the NNW–SSE and the ESE–WNW oriented compressional palaeostress fields, suggest that in the study area both N–S and E–W shortening took place, which could also result in the formation of cogenetic folded structures geometrically corresponding to the palaeostress orientations.

4.2.2. Normal faults

In the study area, extensional stress fields were documented by 26 normal fault planes kinematically grouped into NF1 and NF2 groups (Table 3; Figs. 7, 8). Group NF1 is characterised by N(NW)–S(SE) striking fault planes dipping either towards the NE or SW (with an average dip angle of 60° and 44°, respectively). Kinematic and stress analyses indicated that these 19 measured normal fault planes were formed within a stress field characterized by a P-axis steeply dipping towards the SE (P-axis orientation is 159/61; Table 3, Fig. 7) and a NE–SW trending T-axis which suggests NE–SW extension during formation of the NF1 group.

Normal faults of the NF2 group with NE–SW striking fault planes are characterised by NW (Fig. 8b) and SE dipping fault subsets with average dip angles of 56° (NF2/a) and 40° (NF2/b), respectively. Palaeostress field analysis for the NF2 group indicates that the observed fault planes were formed as a result of NW–SE extension, with the P-axis steeply dipping towards the SE (130/67; see Table 3) and the subhorizontal T-axis trending NW–SE (Table 3; Fig. 7).

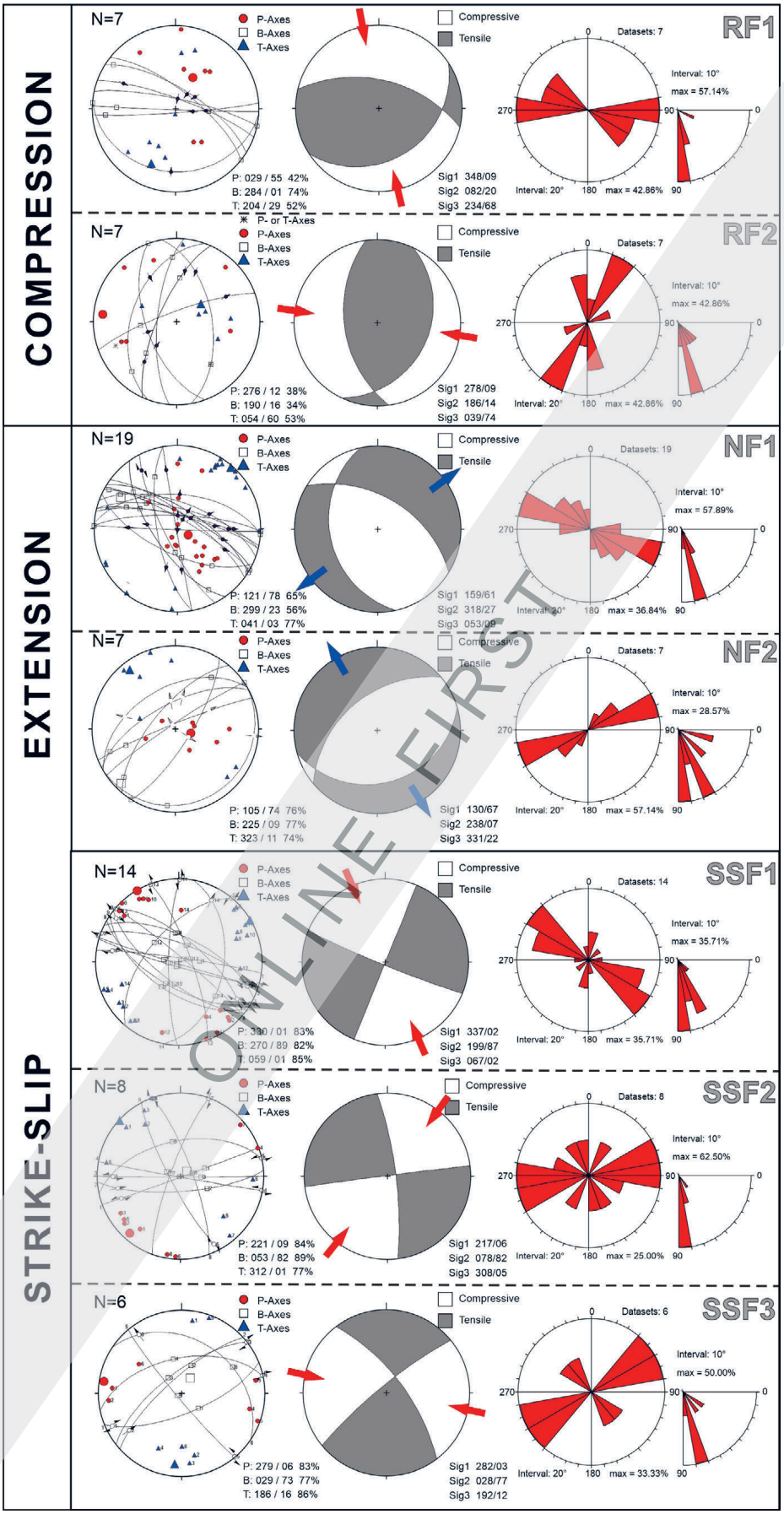

Figure 7. Structural diagrams of fault planes measured in the area of the Northern Velebit National Park and the surrounding area. White quadrants on the beach-ball diagrams represent compressional fields while the grey quadrants represent tensional fields. Measured fault kinematics data indicate compression, extension and strike-slip motions along the measured faults. RF1 and RF2 – reverse fault groups; NF1 and NF2 – normal fault groups; SSF1, SSF2, SSF3 – strike-slip fault groups. The red points, white rectangles, and blue triangles indicate σ1, σ2, and σ3 stress axes, respectively

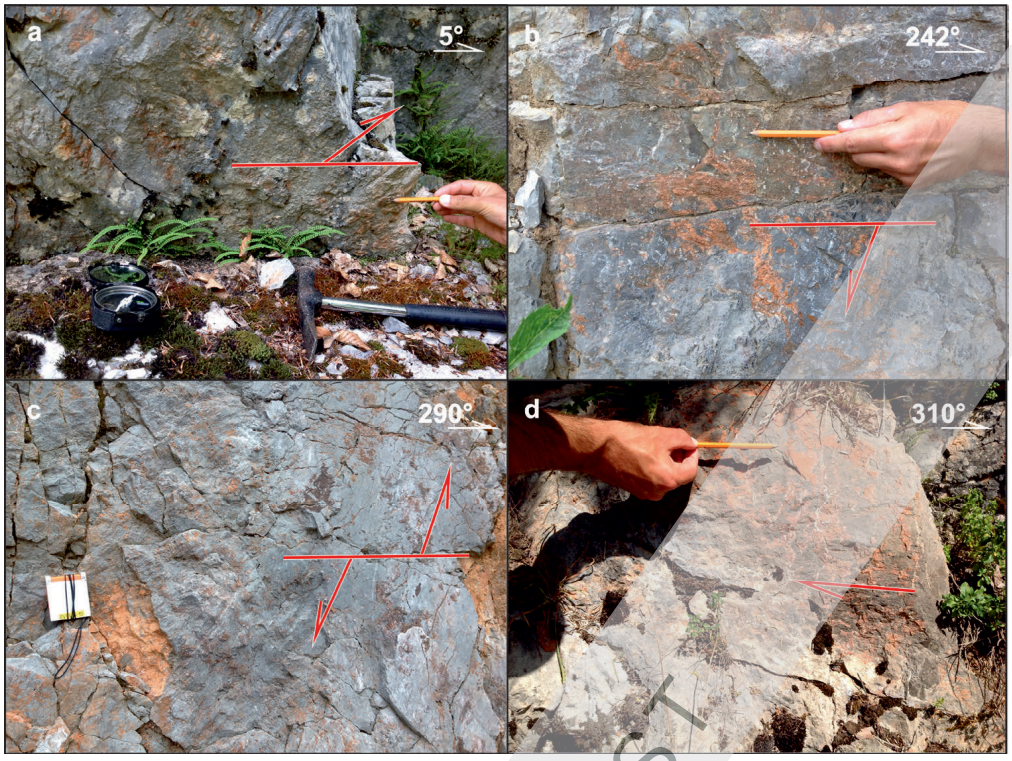

Figure 8. (a) Reverse fault (F-275/71) measured within the Lower Cretaceous limestone. Striations and slickensides indicate reverse displacement with dextral oblique movement (southeastern section of the Northern Velebit National Park, field location SV-90 (44.721°N, 15.055°E); **(b)** Normal fault (F-332/65) measured within Lower Jurassic limestone. Striations and slickensides indicate normal displacement with dextral oblique movement (eastern section of the Northern Velebit National Park, field location SV-78; 44.777°N, 15.102°E); **(c)** Structurally reactivated and inverted reverse fault (F-20/64) measured as a normal fault within the Lower Jurassic limestone. Striations and slickensides indicate both normal and reverse displacement with discrete dextral/sinistral oblique movement (eastern section of the Northern Velebit National Park, field location SV-78; 44.777°N, 15.102°E); **(d)** Dextral fault (F-40/68) measured within Middle Jurassic limestone. Striations and slickensides indicate clear dextral movement (eastern section of the Northern Velebit National Park, field location SV-83; 44.769°N, 15.051°E)

4.2.3. Strike-slip faults

Strike-slip tectonics in the study area are indicated by 28 measured fault planes. Based on geometric properties and fault plane kinematics these faults were subdivided into three principal fault groups, SSF1, SSF2 and SSF3 (Table 3; Figs. 7, 8).

The SSF1 group comprises 14 subvertical fault planes (dip angles between 86° and 89°), dominantly striking either NNE–SSW or ESE–WNW. Associated with the NW–SE trending P-axis (T-axis trending NE–SW; see Fig. 7; Table 3), this palaeostress field resulted in the formation of ESE–WNW striking dextral and NNE–SSW striking sinistral faults. The SSF2 group is composed of eight subvertical fault planes (dip angles between 80° and 89°) with a general N–S and E–W strike (see Table 3). This fault group was associated to a palaeostress field with the NE–SW trending P-axis (T-axis trending NW–SE; see Fig. 7; Table 3) which formed N–S striking dextral and E–W striking sinistral faults. The third strike-slip fault group, the SSF3, comprises six subvertical (dip angles between 74° and 82°) fault planes with a general NE–SW and NW–SE strike. These NW and NE-dipping dextral and sinistral faults (see Figs. 7, 8d) were tectonically active within the palaeostress field with the ESE–WNW trending P-axis (T-axis trending NNE–SSW; see Fig. 7; Table 3).

The studied strike-slip fault planes with subvertical geometry and generally a N–S and E–W strike, locally deviating either towards the NE or NW, were often ambiguously covered by slickenside overgrowths. Slickenside overgrowths and striations indicate repeated sinistral/dextral reactivation which imply re-orientation of the principal stress axes σ1 and σ3, possibly within the same stress field. Furthermore, kinematic/stress analysis within the study area indicates that the SSF1 and SSF2 fault groups were potentially formed in the same palaeostress field associated with the general N–S trending P-axis, which, due to the local stress deviation towards either the NNW (SSF1) or NE (SSF2), yielded recurring dextral/sinistral motions along the faults with similar orientations. Kinematic/stress analysis suggests that the observed SSF3 fault group with NE- and NW-striking fault planes indicate significant palaeostress field re-orientation, from a general N–S trending P-axis (as recorded by SSF1 and SSF2 fault groups) to a dominantly E–W trending P-axis. This suggests regional stress field reorientation combined with structural rotation/translation of faulted structures within the study area.

In this study, field structural relationships, i.e., cross-cutting relationships between the observed fault planes/shear joints, suggest structural reactivation and tectonic inversion of reverse into normal faults (Fig. 8c), followed by the formation of strike-slip faults with both dextral and sinistral movements.

4.3. Geological profiles and structural-stratigraphic relationships

Geological mapping was used to study lithostratigraphic units within the Northern Velebit National Park and the surrounding area, mostly within the area marked as carbonate breccia on

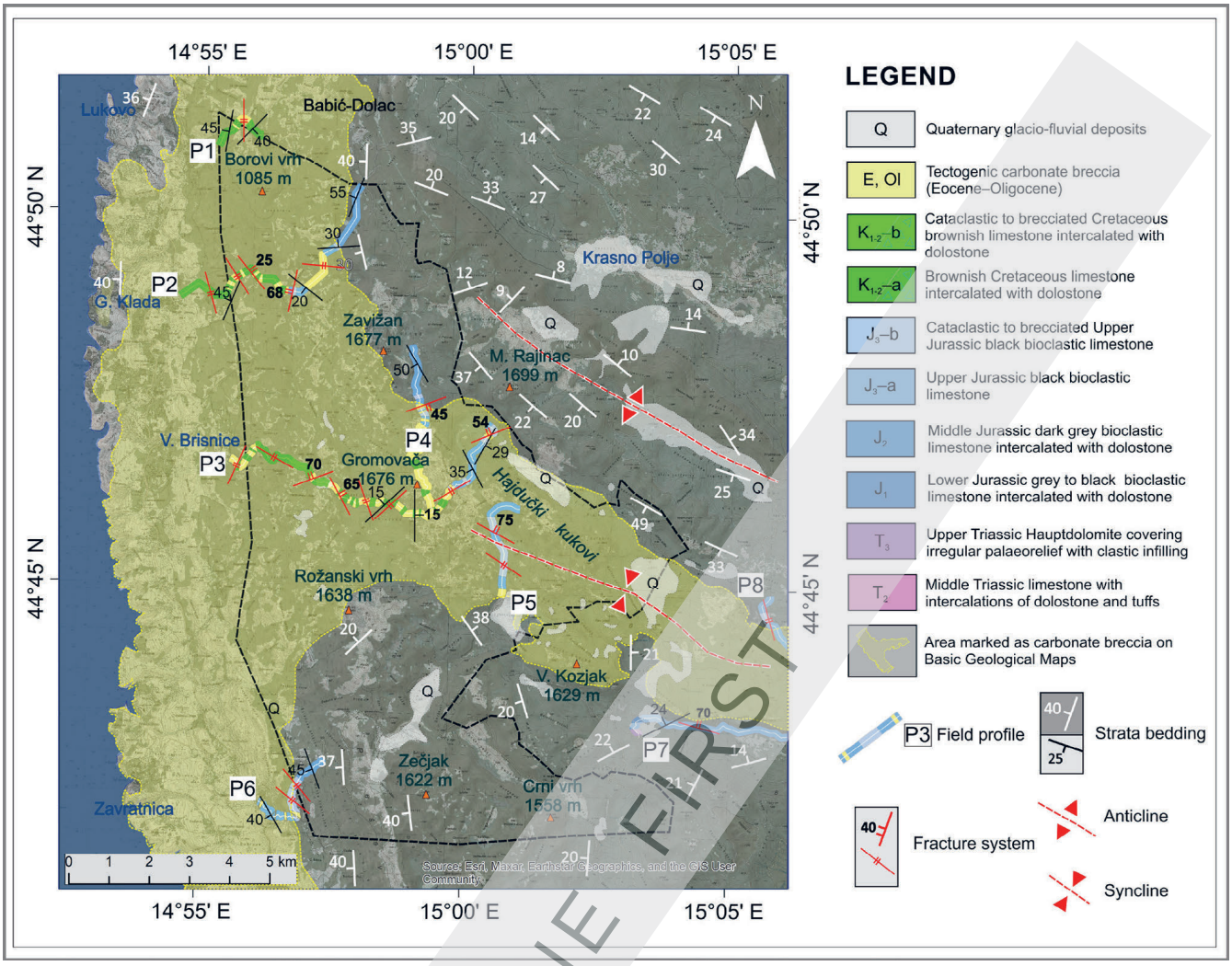

Figure 9. Map of the study area with traces of eight (P1 to P8) profiles along which geological mapping and systematic structural measurements were performed. Determined lithostratigraphical units along the profile lines are indicated with colours and described in the legend, while the typical orientations of bedding and fracture systems are indicated with symbols. White bedding symbols, fault traces and fold axes are adopted from the Basic Geological Maps of the area (MAMUŽIĆ et al., 1969; VELIĆ et al., 1974) and structural data presented in TOMLJENOVIĆ et al. (2017). Dashed black polygon outlines the Northern Velebit National Park area, while the yellow polygon indicates the area marked as being covered by carbonate breccia on the existing Basic Geological Maps of the area (MAMUŽIĆ et al., 1969; VELIĆ et al., 1974)

the existing geological maps (yellow on Figs. 2, 9). The mapping along eight profiles (P1–P8; Figs. 2, 9), showed that the study area is lithologically much more complex than previously thought. Generally, the E–W and N–S oriented P1–P8 profiles indicate that within the area marked as carbonate breccia on the existing maps (MAMUŽIĆ et al., 1969; VELIĆ et al., 1974), a major part is actually covered by Upper Jurassic and Cretaceous limestones (and some dolomites), another part is covered by different lithotypes of the TCB described here and the smallest part by intensely tectonised to brecciated Upper Jurassic and Cretaceous limestones (Fig. 9; Table 4).

The main scope of this study was the study of the TCB, often heavily fractured and tectonised monomictic to polymictic carbonate breccia which is predominantly composed of clasts of the surrounding Cretaceous and Jurassic host rocks (Fig. 10a). Along the mapped profiles, the TCB locally includes clasts of similar but older, cannibalised polymictic carbonate breccia, and some small lenses of breccia-conglomerates, commonly containing rounded extraclasts of younger rocks that today can be found only kilometres or even tens of kilometres from the studied area (Fig. 10b). The presence of conglomerates and breccia-conglomerates within the TCB furthermore indicates the presence of small-scale fluvial systems within the breccia complex.

Geological mapping along the P1–P8 profiles confirmed that approximately two thirds of all profile lengths marked as carbonate breccia on the Basic Geological Maps is actually composed of tectonically relatively undisturbed Jurassic and Cretaceous limestones and some dolomites (Figs. 10c, d; Table 4). Almost 12% of the area along the studied profiles is covered by intensely tectonised and in situ brecciated Upper Jurassic and Lower Cretaceous limestones, often representing crackle/mosaic breccia (Figs. 10e, f) as a gradual transition into the TCB.

The proportion of the TCB studied in this paper varies along the individual profiles from 0% to ≈ 58% of the profile's length, with an average value of around 21.5%. TCB's are usually found as 50 to 800 m wide zones along the profiles characterised

Figure 10. (a) Tectonised polymictic breccia (TCB unit) including clasts of both Cretaceous and Jurassic limestones (central section of the Northern Velebit National Park, along the P3 profile, location SV-332; 44.777°N, 14.947°E); **(b)** A fragment of polymictic breccia-conglomerate (TCB unit) within the predominant tectonised polymictic breccia lithotype (southern section of the Northern Velebit National Park, along the P6 profile, location SV-268; 44.700°N, 14.938°E); **(c)** Homogeneous bioclastic Upper Jurassic limestone (central part of the Northern Velebit National Park, along the P3 profile, location SV-469; 44.779°N, 15.002°E); **(d)** Brownish, homogeneous micritic Lower Cretaceous(?) limestone (central section of the Northern Velebit National Park, along the P4 profile, location SV-512; 44.770°N, 14.989°E); **(e)** Tectonised Upper Jurassic limestone locally reworked into monomictic breccia (central section of the Northern Velebit National Park, along the P4 profile, location SV-493; 44.789°N, 14.986°E); **(f)** Monomictic breccia composed of locally reworked tectonised Upper Cretaceous limestone fragments (southern section of the Northern Velebit National Park, along the P6 profile, location SV-510; 44.769°N, 14.989°E)

by extensively developed karstic landforms (e.g. sinkholes, karstic towers, pits), genetically formed along the dense network of N–S oriented steep to subvertical fracture systems locally deviating to either NW or NE (Figs. 5, 9; Table 2).

Here it should be noted that the percentages of TCB on other potential profiles across the studied area, or other areas comprising such rocks, could be significantly different due to the very pronounced structural and lithological complexity of such areas. Therefore, the presented data should not be taken as representative of the entire Velebit Mt. or other areas covered by similar rocks in the External Dinarides.

Additionally, it is worth mentioning that the transition from both Jurassic and Cretaceous limestones and dolomites to TCB in the Northern Velebit area is predominantly gradual, in the form of a few to tens of metres wide zones and often characterised by a steeply inclined to subvertical geometry. This agrees with observations reported by VLAHOVIĆ et al. (2012) about the tectonic/stratigraphic emplacement of the Velebit breccia within the area of central and southern Velebit. Limestones and dolomites are more common E or W of the central National Park area characterised by predominantly TCB outcrops, and general bedding in such zones is in

Table 4. Geological mapping of the Northern Velebit NP area was performed along eight profiles, P1 to P8. Based on their lithology several informal lithostratigraphical units were separated during the mapping (see Fig. 9), shown here grouped into three distinct units. Their mapped surface coverage along each profile within the area mapped as breccia on the Basic Geological Maps sheets is indicated with the percentage value. Legend of profile names: P1 – Trnovac–Roglić dolina; P2 – Babić-Sića–Gornja Klada; P3 – Velike Brisnice–Livadica; P4 – Zavižan–Rossijeva koliba; P5 – Veliki Lubenovac–Hajdučki Kukovi; P6 – Jablanac–Alan; P7 – Kosinj–Vranjkova Draga; P8 – Kosinjski Bakovac–Mračaj.

Field profile	P1	P2	P3	P4	P5	P6	P7	P8	Cummulative profile length	Percentage (%)
Total field profile length (km)	1.65	7.12	13.12	3.91	2.96	3.86	11.47	14.58	58.87	100
Profile length within the area mapped as breccia in the NP Northern Velebit (km)	1.65	5.46	13.12	2.51	2.96	2.86	1.48	13.58	43.62	74.09
Mapped lithostratigraphic varieties within the area marked as breccia along the profiles										
Lithostratigraphic varieties	Percentage (%)	Percentage (%)	Percentage (%)	Percentage (%)	Percentage (%)	Percentage (%)	Percentage (%)	Percentage (%)	Cummulative profile length	Percentage (%)
Tectogenic carbonate breccia (E, Ol)	20.25	28.37	40.53	57.98	7.45	16.59	–	–	9.35	21.44
Intensely tectonised to brecciated Upper Jurassic and Cretaceous limestones	–	6.78	17.42	6.47	41.46	33.03	–	1.2	5.15	11.81
Triassic–Jurassic–Cretaceous limestone and dolomite succession	79.75	64.85	42.05	35.55	51.09	50.38	100.0	98.8	29.12	66.75

accordance with Jurassic and Cretaceous strata orientation in the wider area, as observed on the geological map of the area (Figs. 2, 9).

4.4. Lithotypes of intensely tectonised carbonates and Tectogenic carbonate breccia

Detailed structural, petrographic and sedimentological observations, of the genetically related intensely tectonised limestones/dolomites and carbonate breccia rock samples collected within the Northern Velebit National Park area (Table 2), enabled distinction of five specific lithotypes. Among these, two represent intensely tectonised carbonates and three belong to the TCB.

The first identified lithotype is composed of intensely tectonised limestones (mostly of Upper Jurassic, partly Cretaceous age; dolomites are relatively rare) in which no displacement or rotation between clasts along numerous fractures was observed, resulting in perfect fitting. Although such outcrops are usually characterised by a relatively massive habitus and intense tectonic deformation, the original bedding or relics of bedding is at least locally still recognisable.

As the intensity of differential stresses progress, the aforementioned intensely tectonised limestones gradually transition into the second lithotype, a crackle/mosaic carbonate breccia (Fig. 11a), in which the individual clasts have experienced some minor displacements and rotations at mesoscale/microscale, the rocks are differentially cemented by calcite, but the fitting between individual clasts is still mostly clearly reconstructable. Outcrops of this lithofacies subtype are usually massive, since the original bedding is often unrecognisable. The intensely tectonised limestones and crackle/mosaic breccia lithotypes appear in transitional zones of varying widths (typically from a few metres to several tens of metres) between homogeneous carbonate successions and TCB.

The third recognisable lithotype belongs to the TCB and represents a monomictic carbonate breccia (Fig. 11b), composed of clasts of neighbouring carbonate rocks (mostly Upper Jurassic dark grey to black coloured limestones). Individual breccia clasts are often intensely tectonised, i.e. crosscut with extensive white calcite veins. Clast sizes are smaller, mostly from millimetres up to 5 cm in size, with only sporadic larger ones. The matrix is composed of finely crushed carbonate material, which is usually lighter in colour than the clasts (Fig. 11b). Such monomictic carbonate breccia occurrences are structurally/texturally unordered and exhibit clear fractalisation.

The fourth lithotype also belongs to the TCB, and it represents a polymictic carbonate breccia (Fig. 11c, d), composed predominantly of clasts of neighbouring limestones, but mixed with variable amounts of limestone clasts of different chronostratigraphic units (which in all documented cases so far, are younger than the neighbouring rocks), including clasts of the Upper Cretaceous rudist and calcisphaera limestones and Palaeogene foraminiferal limestones. Besides the predominant carbonate clasts, locally minor contributions of previously formed monomictic/polymictic breccia fragments and small non-carbonate grains (up to a few millimetres) can be observed. Clasts of neighbouring rocks are typically up to 5–10 cm in size, only exceptionally larger. Clasts of younger chronostratigraphic units (Upper Cretaceous and Palaeogene) are typically coarser, more rounded, and less fractured than the predominant clasts of the Upper Jurassic limestones. Within this lithofacies subtype, two distinct members which cannot be differentiated during geological mapping can be distinguished: a rarely present matrix-supported polymictic breccia (Fig. 11c) and a more common clast-supported polymicitic breccia (Fig. 11d). In the matrix-supported breccias, stratification is locally preserved in the form of vaguely visible clast grading, while clast-supported breccias are generally more massive and chaotic, more tectonised, and commonly penetrated by pressure dissolution forms, i.e. stylolites and dissolution seams. Similar to the monomictic breccia, the polymictic breccia also displays a massive outcrop habitus.

The fifth lithotype which also belongs to the TCB is very rare, and is composed of lenses of carbonate conglomerates

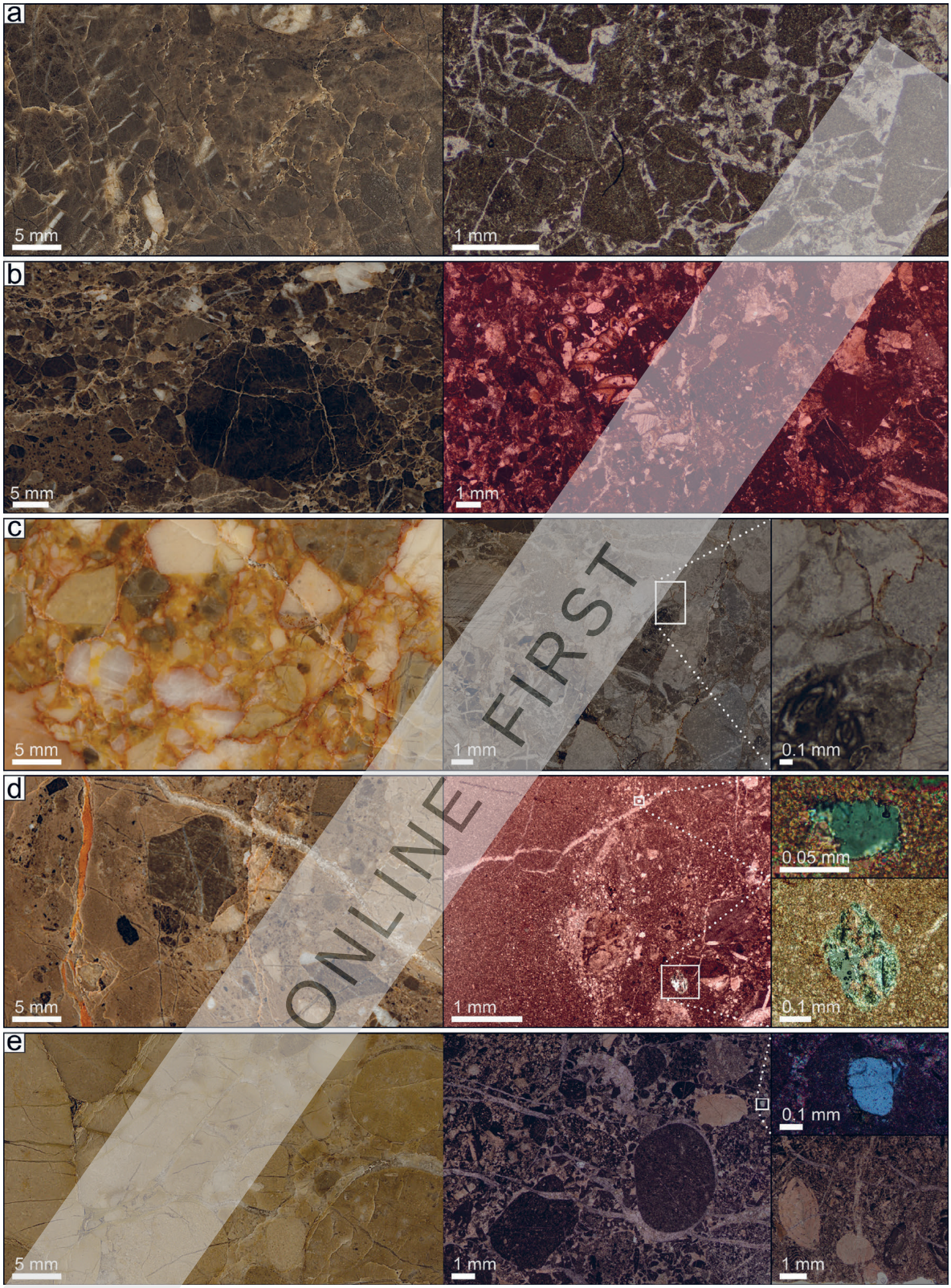

Figure 11. Brecciated limestones and TCB lithofacies subtypes: images on the left are polished slabs, images on the right are thin-section photomicrographs. **(a)** Crackle/mosaic breccia composed of sharp-edged clasts cemented with calcite (sample SV-2-19); **(b)** Monomictic breccia containing darker and lighter clasts of the Upper Jurassic limestones (sample V2-13); **(c)** Clast-supported polymictic breccia composed mostly of Cretaceous clasts and orange-coloured matrix, with stylolitic contacts along clast edges (sample SV-21-19); **(d)** Matrix-supported polymictic breccia with darker Upper Jurassic clasts and lighter, probably Cretaceous clasts, with rare non-carbonate grains in a fine-grained matrix (sample V2-9); **(e)** Polymictic conglomerate composed of Cretaceous and Palaeogene pebbles cemented with calcite with rare quartz grains (sample SV-15-21). Figures b–e represent TCB

and breccia-conglomerates (Fig. 11e), spatially very restricted, both vertically and laterally. This lithotype has only been identified along the P6 profile (Figs. 9, 10b), within the SW part of the Northern Velebit National Park. Conglomerates are mainly composed of clasts originating from younger chronostratigraphic units, Upper Cretaceous micritic to bioclastic

rudist limestones and calcisphaera limestones and Palaeogene foraminiferal limestones. The conglomerate and breccia-conglomerate lithotype is in places characterised by clearly visible stratification marked by gradation or subparallel orientation of elongated clasts, and locally planar discontinuities resembling bedding planes. The clast dimensions are usually up to 10 cm, but in places larger clasts have been observed. Clasts are mostly cemented by calcite.

5. DISCUSSION OF THE STRUCTURAL EMPLACEMENT OF THE TECTOGENIC CARBONATE BRECCIA OUTCROPS IN THE NORTHERN VELEBIT AREA

The tectonic evolution and complexity of the structural emplacement of the Velebit Mt. structure within the External Dinarides has been a research subject for decades. Although it was finally tectonically uplifted during the Middle Eocene–Oligocene due to the Adria Microplate–Euroasian Plate collision, the mechanisms and responsible cogenetic fault systems have not been unambiguously defined. BAHUN (1974), TARI KOVAČIĆ & MRINJEK (1994) and PRELOGOVIĆ et al. (1995, 2004) suggested Eocene–Oligocene uplift along the supposed NE-dipping Velebit reverse fault, which was presumed to lie in the Velebit Channel between the Velebit Mt. and the islands of Rab and Pag. KORBAR (2009, 2025) considered that cogenetic tectonic uplift of the Velebit anticline was caused by the subvertical NE-dipping Cenozoic dextral-reverse fault, which during the Neogene accommodated the final Velebit uplift due to the dextral escape tectonics. The most recent tectonic scenario proposed by BALLING et al. (2021b, 2023) quantitatively documented formation of the Velebit Mt. monocline (see VFZ in Fig. 1), in the hanging wall of the SW-dipping Lika passive backthrust. These authors concluded that the Velebit uplift commenced within an Eocene–Oligocene timeframe, along from Mesozoic inherited and tectonically inverted NE-vergent backthrusts (see geological profile CVP in Fig. 1), that accommodated at least 44 km of horizontal shortening. All three scenarios, though kinematically different, describe exhaustive faulting and folding of the Velebit Mt., followed by intense cogenetic brittle deformation and brecciation of the Mesozoic–Palaeogene predominantly carbonate complex, which yielded formation of the TCB complex.

Due to the extent of Velebit of almost 150 km, this breccia study focused only on the NW portion of the Velebit Mt., mostly within the Northern Velebit National Park (Fig. 2). Although massive TCB outcrops often cover tectonic contacts within the study area, geological mapping and detailed structural investigations clearly indicate the polyphase tectonic evolution. Within the intensively karstified Velebit landscape, bedding measured in Jurassic and Cretaceous carbonate rocks suggests a prevalence of folded structures characterised by gentle folds and N–S (locally NNW–SSE) trending sub-horizontal fold axes (see Figs. 5, 12), formed under an E–W (ENE–WSW) oriented compressional/transpressional stress field. The presence of gentle folds with interlimb angles of between 100° and 130° within the Velebit Jurassic–Cretaceous carbonate complex, suggests the prevalence of stable and relatively low-rate stresses in the area, without subsequent rotation or translation of the folded structures.

At the same time, several hundred measured fracture data within the Jurassic–Cretaceous carbonates and the TCB complex (Fig. 5), provided evidence of carbonate brittle deformation coeval with fracture system formation, which enabled subsequent intense karstification and landscape formation (STEPIŠNIK et al., 2019 and references therein). The fracture system analysis identified six dominant fracture systems mostly striking N–S or slightly deviated either toward the NE or NW. Characterised by their steep geometry (dip angles between 48° and 66°, see Table 3), the delineated fracture systems are mostly concentrated in the central part of the study area (Fig. 9), subparallel to the ≈3 km wide hinge zone of the Northern Velebit anticline (Fig. 12).

Kinematic and stress analysis of the mapped fault planes structurally subparallel to the observed fracture systems, suggested differential stresses within the study area. Based on stress analyses of the kinematically defined fault groups, potentially two compressional phases have been identified within the study area, associated with either NNW–SSE or ESE–WNW oriented compression (Figs. 7, 8). Both contractional phases, though with slightly different orientations of the P-axis, most likely occurred during the Palaeogene, due to the generally N–S oriented Adria Microplate–Eurasian Plate collision (KASTELIC et al., 2013; USTASZEWSKI et al., 2014; SCHMID et al., 2020). Furthermore, ESE–WNW oriented compression probably caused formation of N–S (NNW–SSE) striking folds in the study area (Fig. 5). Either cogenetic with the compressional phases or following closely after, 26 mapped normal faults (Fig. 7) suggest stress field perturbation, causing NE–SW and NW–SE oriented extension of the Northern Velebit area. These extensional structures with similar orientations and geometry to the already existing reverse faults (see Fig. 7) suggest potential tectonic inversion of the previously formed reverse faults in the area, which enabled gravitational collapse and structural relaxation of the Northern Velebit anticline. Extensional structural collapse, common in the orogenic systems (e.g., TAVANI et al., 2012), has already been reported in the NW Dinarides, e.g. in the Vinodol valley and Bakar Bay area, NW of the Northern Velebit, where PALENIK et al. (2019) observed normal faulting as a result of NE–SW, E–W and NW–SE extension within the Cretaceous–Palaeogene folded succession.

Polyphase tectonics of the Northern Velebit area is furthermore documented with measured N–S and E–W striking strike-slip faults, which are characterised by both dextral and sinistral kinematics, i.e., repeated structural reactivation due to the local stress field perturbation (Figs. 7, 8). Combined cross-cutting relationships, slickenside/striation overgrowths and both sinistral and dextral movement indicators (Table 4), suggest general NW–SE/NE–SW and ESE–WNW oriented transpression/transtension in the Northern Velebit area, which commenced within a post-Palaeogene timeframe (TOMLJENOVIĆ et al., 2017; PALENIK et al., 2019), and is active up to recent time as the N–S oriented stress field in the Kvarner–Velebit area (see FMS-DATABASE, 2019; HERAK & HERAK, 2018).

The complexity of repeated structural reactivation of fault and fracture systems, their tectonic inversions and cogenetic deformations, within the framework of the folded structure of the Northern Velebit area, from the Palaeogene (–Early Miocene?) to post Early Miocene time, undoubtedly affected the Jurassic–Cretaceous succession in the area, especially in the intensely folded areas (Fig. 12). In these areas, the Jurassic–Cretaceous carbonate rocks progressively transition into intensely tectonised limestones, (rarely dolomites) and crackle/mosaic carbonate breccias, and finally into monomictic to polymictic carbonate breccias. Probably most of huge number of clasts derived by very intense tectonic activity resulting in brittle deformation of a thick succession of carbonate rocks, formed rockfall deposits infilling the highly dissected palaeorelief after typically short transport, and part of the material was further moved by other mass movement processes including grain flows and debris flows. Such exclusively locally derived clasts originating from neighbouring carbonate rocks formed typical monomictic carbonate breccias. Polymictic breccia are characterised by variable clast composition due to either lithologically different host rocks cropping out along the zone of TCB, or the occasional input of carbonate clasts derived from relatively distant areas (such clasts are often coarser and more rounded than locally derived clasts), due to the temporary activity of small-scale high-energy fluvial systems characterised by the strong discharge of material from weathered uplifted areas. Occasional surges of large quantities of fresh water may also explain rare records of small outcrops of fine-grained pond or lacustrine deposits within the TCB. All types of TCB are characterised by very strong lithification, which usually results in their enhanced resistance to weathering in comparison to neighbouring limestones, therefore commonly showing positive relief. Lithification was promoted by long-lasting circulation of waters oversaturated in respect to calcium

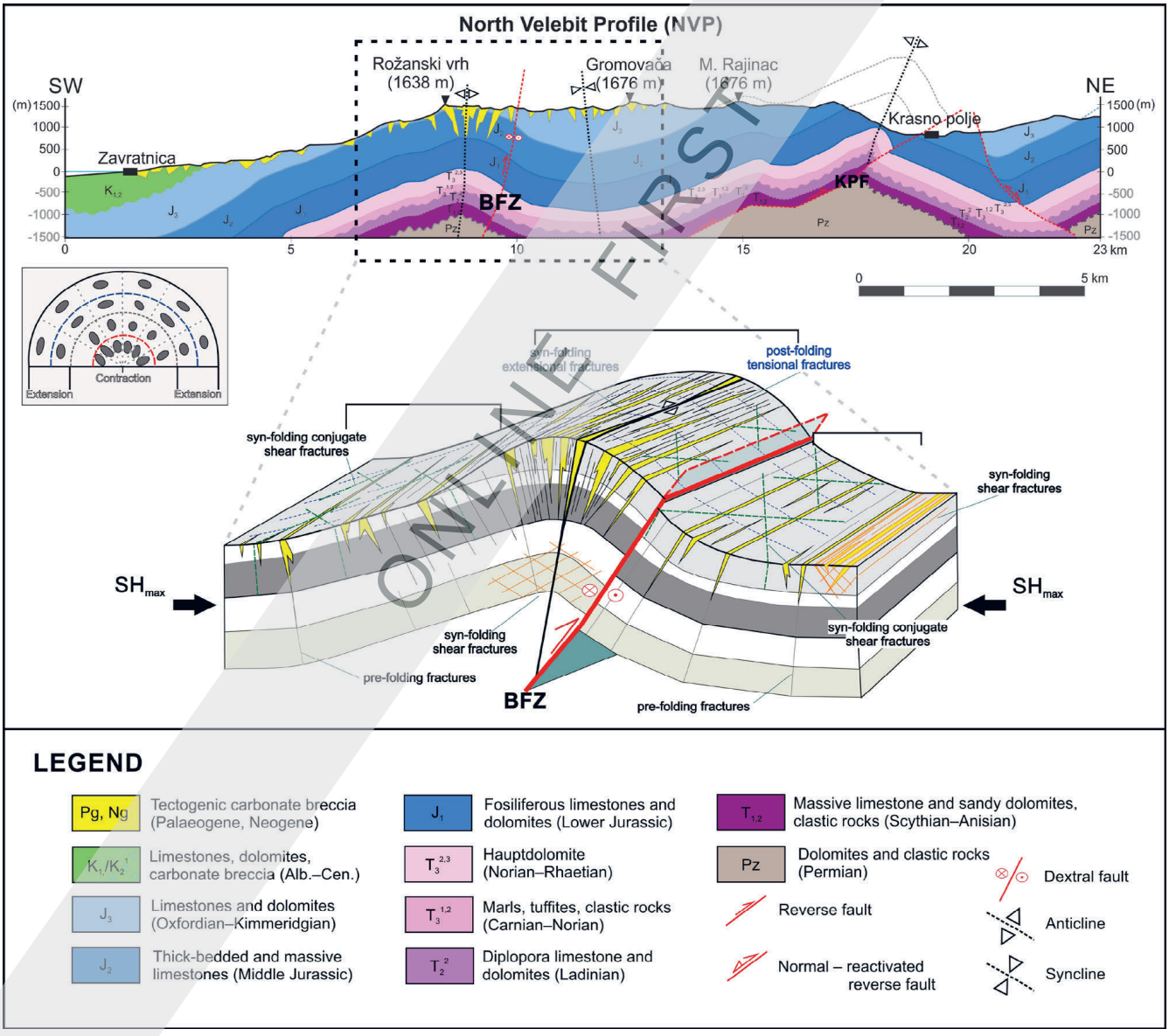

Figure 12. SW–NE oriented Northern Velebit Profile based on geological maps of the studied area (MAMUŽIĆ et al., 1969; VELIĆ et al., 1974) and structural/stratigraphic data collected along the P1–P8 profiles in the Northern Velebit National Park and surrounding area. Structural relationships and TCB emplacement in the area are represented by a schematic model of the fault-related fold with spatial distribution of cogenetic fracture systems. Fracture systems and fault types are defined according to the strain distribution in the fold hinge zones and its limbs. BFZ – Bakovac Fault Zone, KPF – Krasno Polje Fault. Schematic model and strain distribution model modified after RAMSAY & HUBER (1987), TWISS & MOORES (1992), and LI et al. (2018)

carbonate due to the intense karstification in the near-surface zone, during the prolonged subaerial exposure of a tectonically deformed rock complex, composed of carbonates and a huge number of tectonically derived carbonate clasts.

Geological mapping along the eight profiles within the Northern Velebit area (Figs. 2, 3, 9), show considerable structural and textural lithological differences within the area, that according to the available geological maps should be predominantly composed of carbonate breccias (Figs. 2, 9; see MAMUŽIĆ et al., 1969; VELIĆ et al., 1974). Based on geological mapping along the profiles, we differentiated large areas composed of homogenous Jurassic and Cretaceous carbonate rocks, and less spacious outcrops of five lithotypes characterised by intense tectonic influence, from intensely tectonised limestones, crackle/mosaic carbonate breccia, to monomictic and polymictic carbonate breccia and rare carbonate conglomerates and breccia-conglomerates (Figs. 9, 10, 11). Field observations suggested that most transitions between lithotypes are gradual, but mostly steep to subvertical. Most of the monomictic and polymictic breccia and breccia-conglomerates were cropping out in the central part of the Northern Velebit National Park area (Figs. 9, 12), while intensely tectonised limestones and crackle/mosaic breccia dominantly cover the eastern and western portions of the study area, where the TCB complex transitions into less tectonised Upper Jurassic and Cretaceous carbonate successions (Fig. 9). Detailed geological mapping along the P1–P8 profiles, suggested that only 0 to 58% of the individual profile lengths (approximately 21.5% on average), marked as carbonate breccia on Basic Geological Maps is actually composed of TCB, i.e. monomictic to polymictic carbonate breccias, with rare lenses of carbonate conglomerates and breccia-conglomerates (Table 4). Such a considerable discrepancy between breccia area represented on sheets of the Basic Geological Map and the results presented here, may be caused by i) better outcrop accessibility along the newly built/opened trails in the area, and ii) much more detailed and very time-consuming field work along profiles specifically focused on lithological composition along the profile lines. During geological mapping campaigns for the Basic Geological Map, entire zones between the first and last occurrence of massive breccia along the profiles made perpendicular to the profile strike were marked as carbonate breccia due to the very complicated relationships characterised by frequent lithological changes, mostly unrecognisable lithology on the weathered rock surface, as well as a very restricted time available for mapping. Therefore, areas marked as carbonate breccia on the Basic Geological Maps in 1:100,000 scale should be generally considered only as being partly composed of TCB and accompanying intensely tectonised and brecciated carbonate rocks, while a significant part is probably composed of host rocks, mostly limestones and dolomites of different stratigraphic ages, as in other parts of the External Dinarides.

The conducted geological and structural investigations indicate that spatial occurrences of TCB are mostly related to the hinge zone of the NE-verging Northern Velebit anticline structure, characterised by the deep and dense network of NW–SE striking fracture and fault systems (see STROJ & VELIĆ, 2015 for details). Both are tectonically associated with the NNW–SSE striking subvertical fault, a terminal fault strand of the regional NW–SE striking dextral Bakovac Fault Zone (see Figs. 2, 12). Furthermore, in respect to the observed fault kinematic properties, fracture systems and variable tectonised to brecciated rocks within the Northern Velebit area, we may conclude that Palaeogene (–Early Miocene?) and post-Early Miocene tectonic activity resulted in prolonged and recurring hydraulic fracturing, cataclasis and brecciation, with continuous in situ cementation and grinding of sharp angular clasts. Those processes enabled continuous and long-lasting surface and subsurface production of TCB in the area, both monomictic and polymictic, having the surrounding fractured carbonates and partly pre-existing breccia deposits as a source material (see STROJ & VELIĆ, 2015 for details). Rare occurrences of carbonate conglomerates and breccia-conglomerates (Figs. 10b, 11e) within the TCB deposits suggest a highly dissected landscape at the time of deposition, probably characterised by the occasional influence of small-scale fluvial systems of high energy and strong discharge. The presence of TCB occurrences along the SW and NE slopes of the Northern Velebit structure (Fig. 12), out of the hinge zone, adds to the breccia formation complexity in the area, and may indicate that at least part of the breccia deposition could be caused by gravitational redeposition processes. Here, we documented that TCB occurrences are related to the NE-verging Northern Velebit anticline and intense NW–SE striking fracturing and faulting along the NNW–SSE striking subvertical fault (fault strand of the NW–SE striking dextral Bakovac Fault Zone; Fig. 2), which supports a view that massive occurrences of the TCB in the External Dinarides (known in Croatian literature as Jelar/Velebit breccia) represent a unique regional lithofacies found exclusively along the NE-vergent structures, exactly the opposite to most of the structures in the External Dinarides characterised by SW oriented tectonic transport (VLAHOVIĆ et al., 2012; BALLING et al., 2021b, 2023). This cogenetic relationship further proves the complexity of collisional processes along the eastern Adria Microplate margin and indicates a need for detailed study of other TCB occurrences in the area of the External Dinarides, as well as their tectono-sedimentological relationships to the youngest Late Eocene–Oligocene molasse-type Promina beds.

6. CONCLUSION

The Northern Velebit as part of the Velebit Mt. was formed by the Palaeogene (–Early Miocene?) collision of the Adria Microplate and Euroasian Plate. As part of the External Dinarides this ≈150 km long NW–SE striking anticline structure composed of a Late Palaeozoic–Mesozoic to middle to late Eocene (–Oligocene?) carbonate-clastic succession, is partly covered by extensive outcrops of carbonate breccia, i.e., Tectogenic carbonate breccia (TCB), which in the Croatian literature is known as the Jelar deposits (or Jelar formation, Jelar beds, Jelar breccia) or Velebit breccia. In this study, the aims were to (i) identify the structural and tectonic properties of the Northern Velebit area since breccia deposits are caused by intense tectonic processes, and (ii) identify differences between different TCB lithotypes and accompanied intensely tectonised carbonate rocks with respect to their spatial emplacement.

Results of the structural investigations show that the Jurassic–Cretaceous carbonates in the Northern Velebit area form a folded structure with a N–S (locally NNW–SSE) oriented fold axis, probably formed within the E–W (ENE–WSW) oriented compressional/transpressional stress field, during the Palaeogene (–Early Miocene?). Being cogenetic with the fold structure, most of the observed fracture systems show a N–S (locally deviated towards NE or NW) orientation, subparallel with the hinge zone of the Northern Velebit anticline. This gentle, NE-verging fold is formed in the hangingwall of the NNW terminal fault strand of the NW–SE striking dextral Bakovac Fault Zone.

Kinematic and stress analysis of the mapped fault planes supports the observed structural properties, suggesting polyphase tectonic activity. Measured reverse faults suggest the prevalence of a compressional phase with either a NNW–SSE or ESE–WNW oriented P-axis, while similarly oriented normal faults suggest stress field perturbation, and NE–SW and NW–SE extension within the Northern Velebit area. Both fault groups, due to their similar orientations and geometry, suggest structural reactivation and potential tectonic inversion which from the initial Palaeogene (–Early Miocene?) compression, transitioned to post-Early Miocene gravitational extension and structural relaxation of the Northern Velebit anticline. Continuous tectonic activity during the Neogene and Quaternary is evidenced by N–S and E–W striking dextral/sinistral faults which indicate NW–SE/NE–SW and ESE–WNW oriented transpression/transtension.

Identification of the structural emplacement properties of the TCB complex was enabled by geological mapping along eight profiles. Polyphase tectonic evolution is evidenced by sporadic findings of cannibalised older breccia clasts within the younger breccia, as well as by the distribution of different lithotypes related to polyphase tectonic activity within the Northern Velebit anticline, mostly associated to the observed subvertical fracture systems. The Northern Velebit area is characterised by five lithotypes characterised by the gradual transition from the predominant homogenous carbonate rocks of various stratigraphic ages to (1) intensely tectonised limestones, (2) crackle/mosaic carbonate breccia, and three TCB lithotypes – (3) monomictic carbonate breccia, (4) polymictic carbonate breccia, and locally (5) lenses of carbonate conglomerates and breccia-conglomerates.

Field observations and geological mapping suggested that most monomictic to polymictic breccia outcrops and zones are concentrated within the central part of the Northern Velebit area, alternating with tectonised limestones and crackle/mosaic breccia. Towards the NE and SW parts of the study area, in the limbs of the Northern Velebit anticline, predominant tectonised limestones and crackle/mosaic breccia with rare monomictic to polymictic breccia outcrops gradually transition into thick successions of less tectonised carbonate rocks typical for External Dinarides. With only 21.5% on average of the studied profile length (0 to 58% of length along individual profiles) covered by the TCB and an additional, almost 12% of profile length covered by intensely tectonised and brecciated Upper Jurassic and Cretaceous carbonate rocks, it is clear that approximately two thirds of the area marked as carbonate breccia on the existing geological maps of the study area is actually composed of limestones (and less frequently dolomites) of the Upper Jurassic and Cretaceous age. Therefore, we suggest that the future geological mapping of the areas marked as being covered by breccia on the existing Basic Geological Maps of the Velebit Mt. and other areas (e.g. our ongoing studies already indicated some previously unknown occurrences of TCB in different areas of the External Dinarides), should be focused on i) identification of Tectogenic carbonate breccia occurrences with all their lithological variabilities, ii) determination of their relationship with the accompanying intensely tectonised and brecciated carbonate host rocks as well as their clear distinction from typical Mesozoic limestones and dolomites, and iii) recognition of the local tectonic framework resulting in intense tectonic deformation and formation of TCB and accompanied intensely tectonised and brecciated carbonate rocks.

Future additional detailed studies of the TCB in different areas of the External Dinarides should result in the final formalisation of that complex lithostratigraphical unit, using either previously used names for such deposits (the most common being the Jelar or Velebit breccia), with their combination as probably the best compromise (Jelar/Velebit breccia), or any new, better term.

ACKNOWLEDGEMENT

This study was financially supported by the Northern Velebit National Park Public Institution (Project No. 311100022). We are grateful to the National Park services for providing extensive logistical support during field investigations. We thank Prof. Bruno Tomljenović and Assist. Prof. David Rukavina (University of Zagreb, Faculty of Mining, Geology and Petroleum Engineering), and Branimir Šajatović (Northern Velebit National Park) for participating in some field investigations. The authors are grateful to two anonymous reviewers for their very constructive and detailed reviews, which greatly improved the manuscript.

REFERENCES

ALLMENDINGER, R.W., CARDOZO, N. & FISHER, D.M. (2011): Structural Geology Algorithms: Vectors and Tensors.– Cambridge University Press, 289 p. https://doi.org/10.1017/CBO9780511920202

ALJINOVIĆ, D., ISOZAKI, Y. & SREMAC, J. (2008): The occurrence of giant bivalve Alatoconchidae from the Yabeina zone (Upper Guadalupian, Permian) in European Tethys.– Gondwana Research, 13/3, 275–287. https://doi.org/10.1016/j.gr.2007.09.002

ANGELIER, J. & MECHLER, P. (1977): Sur une methode graphique de recherche des contraintes principales egalement utilisables en tectonique et en seismologie: la methode des diedres droits.– Bulletin de la Société Géologique de France S7-XIX, 1309–1318. https://doi.org/10.2113/gssgfbull.S7-XIX.6.1309

BAHUN, S. (1962): Vapnenci Promina-naslaga u području Kruščice u Lici [*Limestones in the Promina deposits of the territory of Kruščica in Lika* – in Croatian with English abstract].– Geološki vjesnik 15, 101–106.

BAHUN, S. (1963): Geološki odnosi okolice Donjeg Pazarišta u Lici (trijas i tercijarne Jelar-naslage) [*Geological relations of the surroundings of Donje Pazarište in Lika (Croatia)* – in Croatian with English abstract].– Geološki vjesnik, 16, 161–170.

BAHUN, S. (1974): Tektonogeneza Velebita i postanak Jelar-naslaga [*The tectonogenesis of Mt. Velebit and the formation of Jelar deposits* – in Croatian with English abstract].– Geološki vjesnik, 27, 35–51.

BAHUN, S. (1984): The tectonic and hydrogeologic significance of the areas composed of the Jelar formation [*Hydrogeological properties of Jelar deposits, Lika (Croatia)* – in Croatian with English abstract].– Carsus Iugoslaviae, 11/1, 1–11.

BAHUN, S. (1985): Trijaske naslage i Jelar-formacija u dolini Une između Srba i Brotnje (Hrvatska) [*Triassic deposits and Jelar Formation in the Una Valley between Srb and Brotnja (Croatia)* – in Croatian with English abstract].– Geološki vjesnik, 38, 21–30.

BALLING, P., GRÜTZNER, C., TOMLJENOVIĆ, B., SPAKMAN, W. & USTASZEWSKI, K. (2021a): Post-collisional mantle delamination in the Dinarides implied from staircases of Oligo-Miocene uplifted marine terraces.– Scientific Reports, 11, 2685, 1–12. https://doi.org/10.1038/s41598-021-81561-5

BALLING, P., TOMLJENOVIĆ, B., SCHMID, S.M. & USTASZEWSKI, K. (2021b): Contrasting along-strike deformation styles in the central External Dinarides assessed by balanced cross-sections: Implications for the tectonic evolution of its Paleogene flexural foreland basin system.– Global and Planetary Change, 205, 103587, 1–24. https://doi.org/10.1016/j.gloplacha.2021.103587

BALLING, P., TOMLJENOVIĆ, B., HERAK, Ma. & USTASZEWSKI, K. (2023): Impact of mechanical stratigraphy on deformation style and distribution of seismicity in the central External Dinarides: a 2D forward kinematic modelling study.– Swiss Journal of Geosciences, 116/7, 30 p. https://doi.org/10.1186/s00015-023-00437-0

BOGNAR, A., FAIVRE, S. & PAVELIĆ, J. (1991): Tragovi oledbe na Sjevernom Velebitu ?Glaciation traces on the North Velebit – in Croatian with English abstract ?.– Croatian Geographical Bulletin, 53, 27–38.

CAPORALI, A., AICHHORN, C., BARLIK, M., BECKER, M., FEJES, I., GERHATOVA, L., GHITAU, D., GRENERCZY, G., HEFTY, J., KRAUSS, S., MEDAK, D., MILEV, G., MOJZES, M., MULIC, M., NARDO, A., PESEC, P., RUS, T., SIMEK, J., SLEDZINSKI, J., SOLARIC, M., STANGL, G., STOPAR, B., VESPE, F. & VIRAG, G. (2009): Surface kinematics in the Alpine–Carpathian–Dinaric and Balkan region inferred from a new multi-network GPS combination solution.– Tectonophysics, 474, 295–321. https://doi.org/10.1016/j.tecto.2009.04.035

CARDOZO, N. & ALLMENDINGER, R.W. (2013): Spherical projections with OSXStereonet.– Computers and Geosciences, 51, 193–205. https://doi.org/10.1016/j.cageo.2012.07.021

CRNOLATAC, I. & MILAN, A., (1959): Prilog poznavanju Prominskih naslaga Like ?Ein Beitrag zur Kenntnis der Prominaschichten in der Lika – in Croatian with German abstract)?.– Geološki vjesnik, 12, 49–52.

CVIJIĆ, J. (1893): Das Karstphänomen: Versuch einer Morphologischen Monographie.– Hölzel, Wien.

D'AGOSTINO, N., AVALLONE, A., CHELONI, D., D'ANASTASIO, E., MANTENUTO, S. & SELVAGGI, G. (2008): Active tectonics of the Adriatic region from GPS and earthquake slip vectors.– Journal of Geophysical Research–Solid Earth, 113, B12: B12413. https://doi.org/10.1029/2008JB005860

DOBLAS, M. (1998): Slickenside kinematic indicators.– Tectonophysics, 295, 187–197. https://doi.org/10.1016/S0040-1951(98)00120-6

FIO, K., SPANGENBERG, J.E., VLAHOVIĆ, I., SREMAC, J., VELIĆ, I. & MRINJEK, E. (2010): Stable isotope and trace element stratigraphy across the Permian–Triassic transition: A redefinition of the boundary in the Velebit Mountain, Croatia.– Chemical Geology, 278/1–2, 38–57. https://doi.org/10.1016/j.chemgeo.2010.09.001

FLUDE, S., BOND C.E. & BUTLER, R.W.H. (2025): Are geological description practices and classification schemes fit for future use? Breccias as an example.– Earth-Science Reviews, 266, 105140. https://doi.org/10.1016/j.earscirev.2025.105140

FMS-DATABASE (2019): Database of Focal Mechanism Solutions.– Unpublished report, Department of Geophysics, Faculty of Science, University of Zagreb.

FRITZ, F. & PAVIČIĆ, A. (1975): Tektonski odnosi u području krednih i Jelar naslaga (tercijar) kod Kosinja u Lici ?Tectonical pattern of Cretaceous and Jelar deposits (Tertiary) at Kosinj, Lika (Croatia) – in Croatian with English abstract?.– Geološki vjesnik, 28, 35–42.

FRITZ, F., BAHUN, S. & PAVIČIĆ, A. (1978): Tektonski okvir karbonatnih klastita u području Zrmanje uzvodno od Obrovca ?Tectonic setting of carbonate clastic sediments in the area of river Zrmanja upstream of Obrovac – in Croatian with English abstract?.– Carsus Iugoslaviae, 9, 273–282.

GOVORČIN, M., HERAK, Ma., MATOŠ, B., PRIBIČEVIĆ, B. & VLAHOVIĆ, I. (2020): Constraints on complex faulting during the 1996 Ston–Slano (Croatia) earthquake inferred from the DInSAR, seismological and geological observations.– Remote Sensing, 12, 1157. https://doi.org/10.3390/rs12071157

GRENERCZY, G., SELLA, G., STEIN, S. & KENYERES, A. (2005): Tectonic implications of the GPS velocity field in the northern Adriatic region.– Geophysical Research Letters, 32, L16311. https://doi.org/10.1029/2005GL022947

GRIMANI, I., ŠIKIĆ, K. & ŠIMUNIĆ, A. (1972): Osnovna geološka karta SFRJ 1:100 000, list Knin L 33-141 ?Basic Geological Map of SFRY 1:100 000, Knin sheet L 33-141 – in Croatian].– Institut za geološka istraživanja, Zagreb, Savezni geološki zavod, Beograd.

GRIMANI, I., ŠUŠNJAR, M., BUKOVAC, J., MILAN, A., NIKLER, L., CRNOLATAC, I., ŠIKIĆ, D. & BLAŠKOVIĆ, I. (1973): Osnovna geološka karta SFRJ 1:100 000. Tumač za list Crikvenica L 33-102 [Basic Geological Map of SFRY 1:100 000. Explanatory notes for the Crikvenica sheet L 33-102 – in Croatian].– Institut za geološka istraživanja, Zagreb, Savezni geološki zavod, Beograd, 47 p.

GRIMANI, I., JURIŠA, M., ŠIKIĆ, K. & ŠIMUNIĆ, A. (1975): Osnovna geološka karta SFRJ 1:100 000. Tumač za list Knin L 33-141 [Basic Geological Map of SFRY 1:100 000. Explanatory notes for the Knin sheet L 33-141 – in Croatian].– Institut za geološka istraživanja, Zagreb, Savezni geološki zavod, Beograd, 61 p.

HERAK, Mi. (1959): Geologija Gračačkog polja u Lici.– Geološki vjesnik, 13, 31–56.

HERAK, Mi. & BAHUN, S. (1979): The role of the calcareous breccias (Jelar Formation) in the tectonic interpretation of the High Karst Zone of the Dinarides ?Uloga vapnenačkih breča (Jelar formacija) u tektonskoj interpretaciji Zone visokog krša u Dinaridima?.– Geološki vjesnik, 31, 49–59.

HERAK, Ma. & HERAK, D. (2018): On earthquake locations using the source-specific station corrections in the Kvarner–Velebit region, Croatia.– In: 36th General Assembly of the European Seismological Commission: Book of Abstracts. University of Malta, Valletta, 486–486.

HERAK, D., HERAK, Ma., PRELOGOVIĆ, E., MARKUŠIĆ, S. & MARKULIN, Ž. (2005): Jabuka island (Central Adriatic Sea) earthquakes of 2003.– Tectonophysics, 397, 167–180. https://doi.org/10.1016/j.tecto.2005.01.007

ISOZAKI, Y., ALJINOVIĆ, D. & KAWAHATA, H. (2011): The Guadalupian (Permian) Kamura event in European Tethys.– Palaeogeography, Palaeoclimatology, Palaeoecology, 308/1–2, 12–21. https://doi.org/10.1016/j.palaeo.2010.09.034

IVANOVIĆ, A., VELIĆ, I., SOKAČ, B. & NIKLER, L. (1965): Geologija područja zapadno od Krbavskog polja [Geology of the area west of Krbavsko polje; in Croatian].– Carsus Iugoslaviae, 2, 13–26.

IVANOVIĆ, A., SAKAČ, K., MARKOVIĆ, S., SOKAČ, B., ŠUŠNJAR, M., NIKLER, L. & ŠUŠNJARA, A. (1973): Osnovna geološka karta SFRJ 1:100 000, list Obrovac L 33-140 [Basic Geological Map of SFRY 1:100 000, Obrovac sheet L 33-140 – in Croatian].– Institut za geološka istraživanja, Zagreb, Savezni geološki zavod, Beograd.

IVANOVIĆ, A., SAKAČ, K., SOKAČ, B., VRSALOVIĆ-CAREVIĆ, I. & ZUPANIČ, J. (1976): Osnovna geološka karta SFRJ 1:100 000. Tumač za list Obrovac L 33-140 [Basic Geological Map of SFRY 1:100 000. Explanatory notes for the Obrovac sheet L 33-140 – in Croatian].– Institut za geološka istraživanja, Zagreb, Savezni geološki zavod, Beograd, 61 p.

IVANOVIĆ, A., SIKIRICA, V., MARKOVIĆ, V. & SAKAČ, K. (1977): Osnovna geološka karta SFRJ 1:100 000, list Drniš K 33-9 [Basic Geological Map of SFRY 1:100 000, Drniš sheet K 33-9 – in Croatian].– Institut za geološka istraživanja, Zagreb, Savezni geološki zavod, Beograd.

IVANOVIĆ, A., SIKIRICA, V. & SAKAČ, K. (1978): Osnovna geološka karta SFRJ 1:100 000. Tumač za list Drniš K 33-9 [Basic Geological Map of SFRY 1:100 000. Explanatory notes for the Drniš sheet K 33-9 – in Croatian].– Institut za geološka istraživanja, Zagreb, Savezni geološki zavod, Beograd, 59 p.

KASTELIC, V., VANNOLI, P., BURRATO, P., FRACASSI, U., TIBERTI, M.M. & VALENSISE, G. (2013): Seismogenic sources in Adriatic Domain.– Marine Petroleum Geology, 42, 181–213. https://doi.org/10.1016/j.marpetgeo.2012.08.002

KOCH, F. (1929): Geološka karta Hrvatske, Slavonije i Dalmacije (prilog geološkoj karti Kraljevine Srba, Hrvata i Slovenaca) Karlobag–Jablanac (Zone 27, Col. XII).– Naklada Geol. zav. u Zagrebu. Repr. Vojno geogr. Inst., Beograd.

KORBAR, T. (2009): Orogenic evolution of the External Dinarides in the NE Adriatic region: A model constrained by tectonostratigraphy of Upper Cretaceous to Paleogene carbonates.– Earth-Science Reviews, 96, 296–312. https://doi.org/10.1016/j.earscirev.2009.07.004

KORBAR, T. (2025): Conflicting tectonic interpretations of the central External Dinarides.– Geologia Croatica, 78/3, 257–265. https://doi.org/10.4154/gc.2025.17

LACKOVIĆ, D. (1993): Lukina jama u sjevernom Velebitu – najdublja jama u Hrvatskoj.– Vijesti Hrvatskog geološkog društva, 30, 83–85.

LI, Y., HOU, G., HARI, K.R., NENG, Y., LEI, G., TANG, Y., ZHOU, L., SUN, S. & ZHENG, C. (2018): The model of fracture development in the faulted folds: The role of folding and faulting.– Marine and Petroleum Geology, 89, 243–251. https://doi.org/10.1016/j.marpetgeo.2017.05.025

MAJCEN, Ž. & KOROLIJA, B. (1973): Osnovna geološka karta SFRJ 1:100 000. Tumač za list Zadar L 33-139 [Basic Geological Map of SFRY 1:100 000. Explanatory notes for the Zadar sheet L 33-139 – in Croatian].– Institut za geološka istraživanja Zagreb, Savezni geološki zavod, Beograd, 44 p.

MAJCEN, Ž., KOROLIJA, B., SOKAČ, B. & NIKLER, L. (1970): Osnovna geološka karta SFRJ 1:100 000, list Zadar L 33-139 [Basic Geological Map of SFRY 1:100 000, Zadar sheet L 33-139 – in Croatian].– Institut za geološka istraživanja, Zagreb, Savezni geološki zavod, Beograd.

MAMUŽIĆ, P. & MILAN, A. (1973): Osnovna geološka karta SFRJ 1:100 000. Tumač za list Rab L 33-114 [Basic Geological Map of SFRY 1:100 000. Explanatory notes for the Rab sheet L 33-114 – in Croatian].– Institut za geološka istraživanja, Zagreb, Savezni geološki zavod, Beograd, 39 p.

MAMUŽIĆ, P. & SOKAČ, B. (1973): Osnovna geološka karta SFRJ 1:100 000. Tumač za listove Silba i Molat L 33-126 i L 33-138 [Basic Geological Map of SFRY 1:100 000. Explanatory notes for the Silba and Molat sheet L 33-126 and L 33-138 – in Croatian].– Institut za geološka istraživanja, Zagreb, Savezni geološki zavod, Beograd, 45 p.

MAMUŽIĆ, P., MILAN, A., KOROLIJA, B., BOROVIĆ, I. & MAJCEN, Ž. (1969): Osnovna geološka karta SFRJ 1:100 000, list Rab L 33-114 [Basic Geological Map of SFRY 1:100 000, Rab sheet L 33-114 – in Croatian].– Institut za geološka istraživanja, Zagreb, Savezni geološki zavod, Beograd.

MAMUŽIĆ, P., SOKAČ, B. & VELIĆ, I. (1970): Osnovna geološka karta SFRJ 1:100 000, list Silba L 33-126 [Basic Geological Map of SFRY 1:100 000, Silba sheet L 33-126 – in Croatian].– Institut za geološka istraživanja, Zagreb, Savezni geološki zavod, Beograd.

MARINČIĆ, S., KOROLIJA, B. & MAJCEN, Ž. (1976): Osnovna geološka karta SFRJ 1:100 000, list Omiš K 33-22 [Basic Geological Map of SFRY 1:100 000, Omiš sheet K 33-22 – in Croatian].– Institut za geološka istraživanja, Zagreb, Savezni geološki zavod, Beograd.

MARINČIĆ, S., KOROLIJA, B., MAMUŽIĆ, P., MAGAŠ, N., MAJCEN, Ž., BRKIĆ, M. & BENČEK, Đ. (1977): Osnovna geološka karta SFRJ 1:100 000. Tumač za list Omiš K 33-22 [Basic Geological Map of SFRY 1:100 000. Explanatory notes for the Omiš sheet K 33-22– in Croatian].– Institut za geološka istraživanja Zagreb, Savezni geološki zavod, Beograd, 51 p.

MARRETT, R. & ALLMENDINGER, R.W. (1990): Kinematic analysis of fault-slip data. Journal of Structural Geology 12, 973–986. https://doi.org/10.1016/0191-8141(90)90093-E

MATEŠIĆ, D., MATOŠ, B., BILLI, A., SMERAGLIA, L., FABBI, S., BALAIĆ, L. & VLAHOVIĆ, I. (2023): Cenozoic massive carbonate breccia in the External Dinarides of Croatia: The largest outcrop on the island of Krk.– In: VLAHOVIĆ, I. & MATEŠIĆ, D. (eds.): 36th IAS Meeting of Sedimentology: Abstracts Book. Croatian Geological Society, Zagreb, 517–517.

MÉTOIS, M., D'AGOSTINO, N., AVALLONE, A., CHAMOT-ROOKE, N., RABAUTE, A., DUNI, L., KUKA, N., KOCI, R. & GEORGIEV, I. (2015): Insights on continental collisional processes from GPS data: Dynamics of the peri-Adriatic belts.– Journal of Geophysical Research: Solid Earth, 120, 8701–8719. https://doi.org/10.1002/2015JB012023

MORT, K. & WOODCOCK, N.H. (2008): Quantifying fault breccia geometry: Dent Fault, NW England.– Journal of Structural Geology, 30, 701–709. https://doi.org/10.1016/j.jsg.2008.02.005

MRINJEK, E. (1993): Sedimentology and depositional settings of alluvial Promina beds in Northern Dalmatia, Croatia.– Geologia Croatica, 46/2, 243–261.

ORTNER, H., REITER, F. & ACS, P. (2002): Easy handling of tectonic data: the programs TectonicVB for Mac and TectonicsFP for WindowsTM.– Computers & Geosciences, 28, 1193–1200. https://doi.org/10.1016/S0098-3004(02)00038-9

PALENIK, D., MATIČEC, D., FUČEK, L., MATOŠ, B., HERAK, Ma. & VLAHOVIĆ, I. (2019): Geological and structural setting of the Vinodol Valley (NW Adriatic, Croatia): Insights into its tectonic evolution based on structural investigations.– Geologia Croatica, 72, 179–193. https://doi.org/10.4154/gc.2019.13

POLŠAK, A. (1957): Nova nalazišta Prominskih klastičnih sedimenata u Hrvatskom Primorju ?Neue Fundorte klastischer Prominasedimente in Hrvatsko primorje (im Kroatischen Küstenland) – in Croatian with German abstract?.– Geološki vjesnik, 10, 91–103.

POLŠAK, A., JURIŠA, M., ŠPARICA, M. & ŠIMUNIĆ, A. (1976): Osnovna geološka karta SFRJ 1:100 000, list Bihać L 33-116 [Basic Geological Map of SFRY 1:100 000, Bihać sheet L 33-116 – in Croatian].– Institut za geološka istraživanja, Zagreb, Savezni geološki zavod, Beograd.

POLŠAK, A., CRNKO, J., ŠIMUNIĆ, An., ŠIMUNIĆ, Al., ŠPARICA, M. & JURIŠA, M. (1978): Osnovna geološka karta SFRJ 1:100 000. Tumač za list Bihać L 33-128 [Basic Geological Map of SFRY 1:100 000. Explanatory notes for the Bihać sheet L 33-128 – in Croatian].– Institut za geološka istraživanja, Zagreb, Savezni geološki zavod, Beograd, 52 p.

POLJAK, J. (1938): Promina naslage Velebita i Like.– Vesnik Geološkog Instituta Kraljevine Jugoslavije, 25–33.

PRELOGOVIĆ, E., ALJINOVIĆ, B. & BAHUN, S. (1995): New data on structural relationships in the Northern Dalmatian Dinaride Area.– Geologia Croatica, 48/2, 167–176.

PRELOGOVIĆ, E., PRIBIČEVIĆ, B., IVKOVIĆ, Ž., DRAGIČEVIĆ, I., BULJAN, R. & TOMLJENOVIĆ, B. (2004): Recent structural fabric of the Dinarides and tectonically active zones important for petroleum-geological exploration in Croatia.– Nafta, 55/4, 155–161.

RAMOVŠ, A., HINTERLECHNER-RAVNIK, A., KALENIĆ, M., KARAMATA, S., KOCHANSKY-DEVIDÉ, V., KRSTIĆ, B., KULENOVIĆ, E., MIRKOVIĆ, M., PETKOVSKY, P., SREMAC, J. & TEMKOVA, V. (1990): Stratigraphic correlation forms of the Yugoslav Paleozoic.– Rendiconti della Società Geologica Italiana, 12, 359–383.

RAMSAY, J.G. & HUBER, M. (1987): The Techniques of Modern Structural Geology, Vol. 2: Folds and Fractures.– Academic Press, London, 445–473.

ROGLIĆ, J. (1963): Glaciation of the Dinaric mountains and its effects on the Karst.– In: Report of the 6th International Congress on Karst, Warsaw 1961. Lodź, Panstwowe Wydawnictwo Naukowe, 293–299.

SAKAČ, K., BENIĆ, J., BAHUN, S. & PENCINGER, V. (1993a): Stratigraphic and tectonic position of Paleogene Jelar beds in the Outer Dinarides.– Natura Croatica, 55–72.

SAKAČ, K., ŠINKOVEC, B., DURN, G. & BENIĆ, J. (1993b): Boksiti i Jelar-naslage ?The bauxites and Jelar-Beds – in Croatian with English abstract?.– Rudarsko-geološko-naftni zbornik, 5, 59–64.

SARIKAYA, M.A., STEPIŠNIK, U., ŽEBRE, M., ÇINER, A., YILDIRIM, C., VLAHOVIĆ, I., TOMLJENOVIĆ, B., MATOŠ, B. & WILCKEN, K.M. (2020): Last glacial maximum deglaciation of the Southern Velebit Mt. (Croatia): insights from cosmogenic 36Cl dating of Rujanska Kosa.– Mediterranean Geoscience Reviews, 2, 53–64. https://doi.org/10.1007/s42990-020-00030-9

SCHMID, S.M., BERNOULLI, D., FÜGENSCHUH, B., MATENCO, L., SCHEFER, S., SCHUSTER, R., TISCHLER, M. & USTASZEWSKI, K. (2008): The Alpine–Carpathian–Dinaridic orogenic system: Correlation and evolution of tectonic units.– Swiss Journal of Geosciences, 101/1, 139–183. https://doi.org/10.1007/s00015-008-1247-3

SCHMID, S.M., FÜGENSCHUH, B., KOUNOV, A., MAŢENCO, L., NIEVERGELT, P., OBERHÄNSLI, R., PLEUGER, J., SCHEFER, S., SCHUSTER, R., TOMLJENOVIĆ, B., USTASZEWSKI, K., VAN HINSBERGEN, D.J.J. (2020): Tectonic units of the Alpine collision zone between Eastern Alps and western Turkey.– Gondwana Research, 78, 308–374. https://doi.org/10.1016/j.gr.2019.07.005

SCHUBERT, R.J. (1908): Geologische Spezialkarte der im Reichsrate vertrenen Königreiche und Länder der Österreichisch–Ungarischen Monarchie. Novegradi und Benkovac, 1:75.000 (Zone 29 Col. XIII).– Geol Reichanst., Wien.

SCHUBERT, R.J. (1909): Geologische Spezialkarte der im Reichsrate vertrenen Königreiche und Länder der Österreichisch–Ungarischen Monarchie neu afgennomen und herausgeben durch die k. k. Geologische Reichanstalt. Medak und Sv. Rok, 1:75.000 (Zone 28 Col. XIII).– Geol Reichanst., Wien.

SCHUBERT, R.J. (1920a): Geologische Spezialkarte der im Reichsrate vertrenen Königreiche und Länder der Österreichisch–Ungarischen Monarchie. Knin und Ervenik, 1:75.000 (Zone 29 Col. XIV).– Geol Reichanst., Wien.

SCHUBERT, R.J. (1920b): Geologische Spezialkarte der im Reichsrate vertrenen Königreiche und Länder der Österreichisch–Ungarischen Monarchie. Zara, 1:75.000 (Zone 29 Col. XII).– Geol Reichanst., Wien.

SCHUBERT, R.J. & WAAGEN, L. (1912): Geologische Spezialkarte der im Reichsrate vertrenen Königreiche und Länder der Österreichisch–Ungarischen Monarchie neu afgennomen und herausgeben durch die k. k. Geologische Reichanstalt. Pago, 1:75.000 (Zone 28 Col. XII, SW-Gruppe Nr. 115).– Geol Reichanst., Wien.

SMIRČIĆ, D., KOLAR-JURKOVŠEK, T., ALJINOVIĆ, D., BARUDŽIJA, U., JURKOVŠEK, B. & HRVATOVIĆ, H. (2018): Stratigraphic definition and correlation of Middle Triassic volcaniclastic facies in the External Dinarides: Croatia and Bosnia and Herzegovina.– Jornal of Earth Sciences, 29, 310 864–878. https://doi.org/10.1007/s12583-018-0789-1

SMIRČIĆ, D., ALJINOVIĆ, D., BARUDŽIJA, U. & KOLAR-JURKOVŠEK, T. (2020): Middle Triassic syntectonic sedimentation and volcanic influence in the central part of the External Dinarides, Croatia (Velebit Mts.).– Geological Quarterly, 64, 220–239. https://doi.org/10.7306/gq.1528

SOKAČ, B., NIKLER, L., VELIĆ, I. & MAMUŽIĆ, P. (1974): Osnovna geološka karta SFRJ 1:100 000, list Gospić L 33-127 [Basic Geological Map of SFRY 1:100 000, Gospić sheet L 33-127 – in Croatian].– Institut za geološka istraživanja, Zagreb, Savezni geološki zavod, Beograd.

SOKAČ, B., BAHUN, S., VELIĆ, I. & GALOVIĆ, I. (1976a): Osnovna geološka karta SFRJ 1:100 000. Tumač za list Otočac L 33-115 [Basic Geological Map of SFRY 1:100 000. Explanatory notes for the Otočac sheet L 33-115 – in Croatian].– Institut za geološka istraživanja, Zagreb, Savezni geološki zavod, Beograd, 44 p.

SOKAČ, B., ŠČAVNIČAR, I. & VELIĆ, I. (1976b): Osnovna geološka karta SFRJ 1:100 000. Tumač za list Gospić L 33-127 [Basic Geological Map of SFRY 1:100 000. Explanatory notes for the Gospić sheet – in Croatian].– Institut za geološka istraživanja, Zagreb, Savezni geološki zavod, Beograd, 64 p.

SOKAČ, B., ŠUŠNJAR, M., BUKOVAC, J. & BAHUN, S. (1976c): Osnovna geološka karta SFRJ 1:100 000. Tumač za list Udbina L 33-128 [Basic Geological Map of SFRY 1:100 000. Explanatory notes for the Udbina sheet – in Croatian].– Institut za geološka istraživanja, Zagreb, Savezni geološki zavod, Beograd, 62 p.

STEPIŠNIK, U., STOJILKOVIĆ, B. & HOČEVAR, G. (2019): Geomorfološke značilnosti Severnega Velebita [in Slovenian].– In: STEPIŠNIK, U. (ed.): Dinarski kras: Severni Velebit. Ljubljana, Znanstvena založba Filozofske fakultete, 21–43.

STROJ, A. (2004): Speleomorfološke značajke i geneza jamskog sustava Velebita – Dva Javora ?Speleo-morphological features and the genesis of the cave system Velebita – Dva Javora – in Croatian with English abstract?.– Speleolog, 34, 11–17.

STROJ, A. & VELIĆ, I. (2015): Geološki profil Jamskog sustava Lukina Jama–Trojama na Sjevernom Velebitu.– In: HORVAT, M. & WACHA, L. (eds.): 5th Croatian Geological Congress: Abstracts Book. Zagreb, Croatian Geological Survey, 240–241.

ŚRODOŃ, J., ANCZKIEWICZ, A.A., DUNKL, I., VLAHOVIĆ, I., VELIĆ, I., TOMLJENOVIĆ, B., KAWIAK, T., BANAŚ, M. & VON EYNATTEN, H. (2018): Thermal history of the central part of the Karst Dinarides, Croatia: combined application of clay mineralogy and low-T thermochronology.– Tectonophysics, 744, 155–176, https://doi.org/10.1016/j.tecto.2018.06.016

ŠUŠNJAR, M., BUKOVAC, J., NIKLER, L., CRNOLATAC, I., MILAN, A., ŠIKIĆ, D., GRIMANI, I., VULIĆ, Ž. & BLAŠKOVIĆ, I. (1970): Osnovna geološka karta SFRJ 1:100 000, list Crikvenica L 33-102 [Basic Geological Map of SFRY 1:100 000, Crikvenica sheet L 33-102 – in Croatian].– Institut za geološka istraživanja, Zagreb, Savezni geološki zavod, Beograd.

ŠUŠNJAR, M., SOKAČ, B., BAHUN, S., BUKOVAC, J., NIKLER, L. & IVANOVIĆ, A. (1973): Osnovna geološka karta SFRJ 1:100.000, list Udbina L 33-128 [Basic Geological Map of SFRY 1:100,000, Udbina sheet L 33-128 – in Croatian].– Institut za geološka istraživanja, Zagreb, Savezni geološki zavod, Beograd.

TARI, V. (2002): Evolution of the northern and western Dinarides: a tectonostratigraphic approach.– EGU Stephan Mueller Special Publication Series, 1, 223–236. https://doi.org/10.5194/smsps-1-223-2002

TARI KOVAČIĆ, V. & MRINJEK, E. (1994): The role of Palaeogene clastics in the tectonic interpretation of Northern Dalmatia (Southern Croatia).– Geologia Croatica, 47/1, 127–138.

TAVANI, S., STORTI, F., BAUSÀ, J. & MUÑOZ, A. (2012): Late thrusting extensional collapse at the mountain front of the northern Apennines (Italy).– Tectonics, 31, TC4019, 1–17. https://doi.org/10.1029/2011TC003059

TIŠLJAR, J., VLAHOVIĆ, I., VELIĆ, I. & SOKAČ, B. (2002): Carbonate platform megafacies of the Jurassic and Cretaceous deposits of the Karst Dinarides.– Geologia Croatica, 55/2, 139–170.

TOMLJENOVIĆ, B., BALLING, P., MATOŠ, B., VLAHOVIĆ, I., HERAK, Ma., HERAK, D., BLAŽOK, L., POSARIĆ, D., ŠIROL, A., SCHMID, S.M. & USTASZEWSKI, K. (2017): Kinematic analysis of outcrop-scale joint and fault systems in the Velebit Mt. – implication to tectogenesis and active seismo-tectonics.– In: MARJANAC, Lj. (ed.): 5th Regional Scientific Meeting on Quaternary Geology dedicated to Geological Hazards & Final Conference: LoLADRIA project. Zagreb, Croatian Academy of Sciences and Arts, 69–70.

TURNER, F.J. (1953): Nature and dynamic interpretation of deformation lamellae in calcite of three marbles.– American Journal of Science, 251, 276–298. https://doi.org/10.2475/ajs.251.4.276

TWISS, R.J. & MOORES, E.M. (1992): Structural Geology.– W.H. Freeman and Company, New York, 532 p.

USTASZEWSKI, K., HERAK, Ma., TOMLJENOVIĆ, B., HERAK, D. & MATEJ, S. (2014): Neotectonics of the Dinarides–Pannonian Basin transition and possible earthquake sources in the Banja Luka epicentral area.– Journal of Geodynamics, 82, 52–68. https://doi.org/10.1016/j.jog.2014.04.006

VELIĆ, I. & SOKAČ, B. (1981): Osnovna geološka karta SFRJ 1:100 000, list Ogulin L 33-103 [Basic Geological Map of SFRY 1:100 000, Ogulin sheet L 33-103 – in Croatian].– Geološki zavod – OOUR za geologiju i paleontologiju, Zagreb, Savezni geološki zavod, Beograd.

VELIĆ, I., BAHUN, S., SAKAČ, B. & GALOVIĆ, I. (1974): Osnovna geološka karta SFRJ 1:100 000, list Otočac L 33-115 [Basic Geological Map of SFRY 1:100 000, Otočac sheet L 33-115 – in Croatian].– Institut za geološka istraživanja, Zagreb, Savezni geološki zavod, Beograd.

VELIĆ, I., SOKAČ, B. & ŠĆAVNIČAR, B. (1982): Osnovna geološka karta SFRJ 1:100 000. Tumač za list Ogulin L 33-103 [Basic Geological Map of SFRY 1:100,000. Explanatory notes for the Ogulin sheet L 33-103 – in Croatian].– Institut za geološka istraživanja, Zagreb, Savezni geološki zavod, Beograd, 44 p.

VELIĆ, J., VELIĆ, I. & KLJAJO, D. (2011): Sedimentary bodies, forms and occurences in the Tudorevo and Mirovo glacial deposits of northern Velebit (Croatia).– Geologia Croatica, 64/1, 1–16. https://doi.org/10.4154/GC.2011.01

VELIĆ, J., VELIĆ, I., KLJAJO, D., PROTRKA, K., ŠKRABIĆ, H. & ŠPOLJAR, Z.A. (2017): Geological overview of glacial accumulation and erosional occurrences on the Velebit and the Biokovo Mts., Croatia.– Rudarsko-geološko-naftni zbornik, 32/4, 77–96. https://doi.org/10.17794/rgn.2017.4.8

VLAHOVIĆ, I., TIŠLJAR, J., VELIĆ, I. & MATIČEC, D. (2005): Evolution of the Adriatic Carbonate Platform: Paleogeography, main events and depositional dynamics.– Palaeogeography, Palaeoclimatology, Palaeoecology, 220, 333–360. https://doi.org/10.1016/j.palaeo.2005.01.011

VLAHOVIĆ, I., TIŠLJAR, J., VELIĆ, I. & MATIČEC, D. (2007): Immense Tertiary carbonate Jelar breccia, Dinarides, Croatia: A new view.– In: BUSH, D. (ed.): 2007 GSA Annual Meeting and Exhibition: Abstracts with Programs, 146. Denver, Geological Society of America.

VLAHOVIĆ, I., TIŠLJAR, J., VELIĆ, I., ENOS, P., MATIČEC, D., PLETIKOSIĆ, N., PERKOVIĆ, D., PRTOLJAN, B., VELIĆ, J., MRINJEK, E. & MIKŠA, G. (2011): Tertiary carbonate breccia conundrum in the Karst Dinarides of Croatia: Very massive and very neglected.– In: BÁDENAS, B., AURELL, M. & ALONSO-ZARZA, A.M (eds.): 28th IAS Meeting of Sedimentology. Zaragoza, IAS, 460–460.

VLAHOVIĆ, I., MANDIĆ, O., MRINJEK, E., BERGANT, S., ĆOSOVIĆ, V., DE LEEUW, A., ENOS, P., HRVATOVIĆ, H., MATIČEC, D., MIKŠA, G., NEMEC, W., PAVELIĆ, D., PENCINGER, V., VELIĆ, I. & VRANJKOVIĆ, A. (2012): Marine to continental depositional systems of Outer Dinarides foreland and intra-montane basins (Eocene–Miocene, Croatia and Bosnia and Herzegovina).– Journal of Alpine Geology, 54, 405–470.

VLAHOVIĆ, I., VELIĆ, I., TOMLJENOVIĆ, B., MATOŠ, B. & ENOS, P. (2018): Massive Cenozoic carbonate breccia in the Karst Dinarides of Croatia.– In: NEUBAUER, F., BRENDEL, U. & FRIEDL, G. (eds.): XXI International Congress of the Carpathian Balkan Geological Association (CBGA): Abstracts – Advances of Geology in southeast European mountain belts. Sofia, Geologica Balcanica, Bulgarian Academy of Sciences, 201–201.

WAAGEN, L. (1905): Geologische spezialkarte Veglia und Novi, 1:75.000.– Österreichisch–Ungarischen Monarchie.

WAAGEN, L. (1908): Geologische spezialkarte Cherso und Arbe, 1:75.000.– Österreichisch–Ungarischen Monarchie.

WEBER, J., VRABEC, M., PAVLOVČIČ PREŠEREN, P., DIXON, T., JIANG, Y. & STOPAR, M. (2010): GPS-derived motion of the Adriatic microplate from Istria Peninsula and Po Plain sites, and geodynamic implications.– Tectonophysics, 483, 3–4: 214–222. https://doi.org/10.1016/j.tecto.2009.09.001

WOODCOCK, N.H. & MORT, K. (2008): Classification of fault breccias and related fault rocks.– Geological Magazine, 145/3, 435–440. https://doi.org/10.1017/S0016756808004883

ZUPANIČ, J. (1969): Promina naslage planine Promine ?Promina formation of the Promina Mountain – in Croatian with English abstract?.– Geološki vjesnik, 22, 477–498.

ZEBRE, M., SARIKAYA, M.A., STEPIŠNIK, U., COLUCCI, R.R., YILDIRIM, C., CINER, A., CANDAS, A., VLAHOVIĆ, I., TOMLJENOVIĆ, B., MATOŠ, B. & WILCKEN, K.M. (2021): An early glacial maximum during the last glacial cycle on the northern Velebit Mt. (Croatia).– Geomorphology, 392; 1–22. https://doi.org/10.1016/j.geomorph.2021.107918

Supplement 1. N Velebit NP field locations

Location	Time created	Latitude	Longitude
SV-1	13.07.2015. 16:13:55 CEST	44.831	15.053
SV-2	13.07.2015. 16:36:22 CEST	44.833	15.055
SV-3	13.07.2015. 17:12:06 CEST	44.833	15.058
SV-4	13.07.2015. 17:42:21 CEST	44.830	15.059
SV-5	13.07.2015. 17:59:42 CEST	44.831	15.059
SV-6	13.07.2015. 18:07:43 CEST	44.831	15.059
SV-7	13.07.2015. 18:24:45 CEST	44.826	15.068
SV-8	13.07.2015. 18:43:01 CEST	44.826	15.069
SV-9	13.07.2015. 13:13:29 CEST	44.827	15.105
SV-10	13.07.2015. 16:07:56 CEST	44.832	15.053
SV-11	13.07.2015. 16:24:53 CEST	44.832	15.054
SV-12	13.07.2015. 16:36:40 CEST	44.832	15.054
SV-13	13.07.2015. 17:16:29 CEST	44.829	15.065
SV-14	13.07.2015. 17:28:17 CEST	44.828	15.066
SV-15	13.07.2015. 17:43:30 CEST	44.827	15.067
SV-16	13.07.2015. 17:59:17 CEST	44.830	15.069
SV-17	13.07.2015. 18:04:36 CEST	44.829	15.067
SV-18	13.07.2015. 18:10:18 CEST	44.827	15.067
SV-19	13.07.2015. 18:26:01 CEST	44.826	15.068
SV-20	13.07.2015. 18:43:22 CEST	44.826	15.069
SV-21	14.07.2015. 10:33:28 CEST	44.825	15.068
SV-22	14.07.2015. 10:59:15 CEST	44.824	15.078
SV-23	14.07.2015. 11:16:26 CEST	44.822	15.082
SV-24	14.07.2015. 11:43:48 CEST	44.820	15.083
SV-25	14.07.2015. 13:06:06 CEST	44.826	15.088
SV-26	14.07.2015. 13:49:19 CEST	44.824	15.086
SV-27	14.07.2015. 14:10:30 CEST	44.824	15.083
SV-28	14.07.2015. 15:33:39 CEST	44.817	15.055
SV-29	14.07.2015. 15:48:02 CEST	44.801	15.079
SV-30	14.07.2015. 16:47:21 CEST	44.772	15.124
SV-31	14.07.2015. 17:07:01 CEST	44.769	15.130
SV-32	14.07.2015. 17:27:27 CEST	44.764	15.141
SV-33	14.07.2015. 17:40:02 CEST	44.764	15.142
SV-34	14.07.2015. 17:49:49 CEST	44.763	15.148
SV-35	14.07.2015. 18:00:47 CEST	44.764	15.151
SV-36	14.07.2015. 18:18:08 CEST	44.761	15.160
SV-37	14.07.2015. 18:43:53 CEST	44.749	15.194
SV-38	14.07.2015. 09:33:58 CEST	44.822	15.073
SV-39	14.07.2015. 09:52:42 CEST	44.822	15.073
SV-40	14.07.2015. 10:08:30 CEST	44.825	15.069
SV-41	14.07.2015. 10:23:14 CEST	44.825	15.069
SV-42	14.07.2015. 10:36:19 CEST	44.825	15.068
SV-43	14.07.2015. 11:00:04 CEST	44.824	15.078
SV-44	14.07.2015. 11:15:11 CEST	44.823	15.080
SV-45	14.07.2015. 11:35:36 CEST	44.822	15.082
SV-46	14.07.2015. 11:45:23 CEST	44.821	15.083
SV-47	14.07.2015. 13:22:24 CEST	44.827	15.088

Location	Time created	Latitude	Longitude
SV-48	14.07.2015. 13:31:33 CEST	44.825	15.089
SV-49	14.07.2015. 13:43:33 CEST	44.825	15.088
SV-50	14.07.2015. 13:48:56 CEST	44.824	15.087
SV-51	14.07.2015. 14:11:25 CEST	44.824	15.084
SV-52	14.07.2015. 15:46:07 CEST	44.801	15.080
SV-53	14.07.2015. 16:01:24 CEST	44.798	15.089
SV-54	14.07.2015. 16:58:01 CEST	44.771	15.127
SV-55	14.07.2015. 17:07:20 CEST	44.769	15.130
SV-56	14.07.2015. 17:29:10 CEST	44.764	15.141
SV-57	14.07.2015. 17:42:00 CEST	44.764	15.142
SV-58	14.07.2015. 17:49:19 CEST	44.763	15.148
SV-59	14.07.2015. 17:58:58 CEST	44.764	15.151
SV-60	14.07.2015. 18:19:28 CEST	44.761	15.160
SV-61	14.07.2015. 18:47:32 CEST	44.749	15.194
SV-62	15.07.2015. 11:40:33 CEST	44.814	14.970
SV-63	15.07.2015. 12:16:20 CEST	44.816	14.967
SV-64	15.07.2015. 13:02:18 CEST	44.816	14.965
SV-65	15.07.2015. 13:25:48 CEST	44.818	14.964
SV-66	15.07.2015. 13:58:50 CEST	44.818	14.962
SV-67	15.07.2015. 14:22:08 CEST	44.818	14.960
SV-68	15.07.2015. 16:13:10 CEST	44.823	14.978
SV-69	15.07.2015. 16:35:57 CEST	44.831	14.976
SV-70	15.07.2015. 16:55:37 CEST	44.832	14.975
SV-71	15.07.2015. 17:00:27 CEST	44.833	14.976
SV-72	15.07.2015. 17:18:22 CEST	44.832	14.973
SV-73	16.07.2015. 10:41:11 CEST	44.756	15.088
SV-74	16.07.2015. 11:25:53 CEST	44.757	15.064
SV-75	16.07.2015. 13:15:51 CEST	44.771	15.041
SV-76	16.07.2015. 15:23:13 CEST	44.726	15.048
SV-77	16.07.2015. 08:46:06 CEST	44.801	15.075
SV-78	16.07.2015. 09:10:07 CEST	44.777	15.102
SV-79	16.07.2015. 10:30:59 CEST	44.756	15.088
SV-80	16.07.2015. 11:00:37 CEST	44.756	15.086
SV-81	16.07.2015. 11:23:28 CEST	44.758	15.064
SV-82	16.07.2015. 11:46:45 CEST	44.766	15.054
SV-83	16.07.2015. 12:14:33 CEST	44.769	15.051
SV-84	16.07.2015. 12:43:59 CEST	44.771	15.047
SV-85	16.07.2015. 13:02:38 CEST	44.773	15.044
SV-86	16.07.2015. 13:25:35 CEST	44.768	15.040
SV-87	16.07.2015. 15:19:09 CEST	44.725	15.048
SV-88	16.07.2015. 15:51:43 CEST	44.721	15.047
SV-89	16.07.2015. 16:04:04 CEST	44.718	15.056
SV-90	16.07.2015. 16:10:32 CEST	44.721	15.055
SV-91	17.07.2015. 10:14:25 CEST	44.824	15.053
SV-92	17.07.2015. 10:16:58 CEST	44.824	15.053
SV-93	17.07.2015. 12:11:17 CEST	44.862	14.947
SV-94	17.07.2015.	44.814	14.979

Location	Time created	Latitude	Longitude
SV-95	17.07.2015.	44.814	14.976
SV-96	17.07.2015.	44.814	14.975
SV-97	17.07.2015.	44.815	14.976
SV-98	17.07.2015.	44.816	14.976
SV-99	17.07.2015.	44.816	14.976
SV-100	17.07.2015.	44.815	14.975
SV-101	17.07.2015.	44.815	14.975
SV-102	17.07.2015.	44.809	14.971
SV-103	17.07.2015.	44.812	14.970
SV-104	17.07.2015.	44.812	14.971
SV-105	17.07.2015.	44.812	14.971
SV-106	17.07.2015.	44.812	14.972
SV-107	26.10.2015. 11:58:14 CEST	44.820	14.987
SV-108	26.10.2015. 13:01:52 CEST	44.803	14.981
SV-109	26.10.2015. 13:19:32 CEST	44.799	14.984
SV-110	26.10.2015. 13:30:10 CEST	44.798	14.984
SV-111	26.10.2015. 13:38:57 CEST	44.797	14.984
SV-112	26.10.2015. 13:45:30 CEST	44.795	14.983
SV-113	26.10.2015. 13:50:30 CEST	44.794	14.984
SV-114	26.10.2015. 13:53:49 CEST	44.793	14.984
SV-115	26.10.2015. 14:10:28 CEST	44.793	14.984
SV-116	26.10.2015. 14:25:09 CEST	44.791	14.985
SV-117	26.10.2015. 14:38:04 CEST	44.787	14.987
SV-118	26.10.2015. 14:54:14 CEST	44.786	14.985
SV-119	26.10.2015. 15:02:08 CEST	44.785	14.985
SV-120	26.10.2015. 15:18:31 CEST	44.784	14.985
SV-121	26.10.2015. 15:31:48 CEST	44.782	14.986
SV-122	26.10.2015. 15:40:25 CEST	44.780	14.986
SV-123	26.10.2015. 15:52:54 CEST	44.779	14.983
SV-124	26.10.2015. 16:05:49 CEST	44.778	14.984
SV-125	26.10.2015. 16:11:10 CEST	44.777	14.985
SV-126	26.10.2015. 16:26:25 CEST	44.775	14.985
SV-127	26.10.2015. 16:39:16 CEST	44.773	14.987
SV-128	26.10.2015. 16:49:11 CEST	44.771	14.988
SV-129	27.10.2015. 10:43:28 CEST	44.719	14.973
SV-130	27.10.2015. 10:55:21 CEST	44.721	14.973
SV-131	27.10.2015. 11:05:19 CEST	44.722	14.971
SV-132	27.10.2015. 11:16:53 CEST	44.725	14.972
SV-133	27.10.2015. 11:32:19 CEST	44.726	14.969
SV-134	27.10.2015. 11:38:03 CEST	44.728	14.969
SV-135	27.10.2015. 11:52:44 CEST	44.728	14.973
SV-136	27.10.2015. 12:05:44 CEST	44.731	14.973
SV-137	27.10.2015. 12:18:44 CEST	44.733	14.973
SV-138	27.10.2015. 12:31:35 CEST	44.735	14.973
SV-139	27.10.2015. 12:44:24 CEST	44.736	14.975
SV-140	27.10.2015. 12:59:23 CEST	44.738	14.975
SV-141	27.10.2015. 13:05:44 CEST	44.739	14.976
SV-142	27.10.2015. 13:20:10 CEST	44.741	14.976

Location	Time created	Latitude	Longitude
SV-143	27.10.2015. 13:35:44 CEST	44.745	14.977
SV-144	27.10.2015. 13:51:36 CEST	44.747	14.983
SV-145	27.10.2015. 14:01:20 CEST	44.748	14.987
SV-146	27.10.2015. 14:07:07 CEST	44.749	14.990
SV-147	27.10.2015. 14:18:44 CEST	44.750	14.991
SV-148	27.10.2015. 14:43:36 CEST	44.753	14.991
SV-149	27.10.2015. 14:58:02 CEST	44.754	14.989
SV-150	27.10.2015. 15:16:01 CEST	44.757	14.990
SV-151	27.10.2015. 15:26:28 CEST	44.758	14.989
SV-152	27.10.2015. 15:38:29 CEST	44.760	14.989
SV-153	27.10.2015. 15:56:00 CEST	44.762	14.987
SV-154	27.10.2015. 16:06:43 CEST	44.764	14.988
SV-155	27.10.2015. 16:23:56 CEST	44.766	14.989
SV-156	27.10.2015. 10:59:21 CEST	44.731	14.997
SV-157	27.10.2015. 11:10:14 CEST	44.734	15.002
SV-158	27.10.2015. 11:27:39 CEST	44.735	15.006
SV-159	27.10.2015. 11:49:48 CEST	44.739	15.009
SV-160	27.10.2015. 12:13:56 CEST	44.739	15.012
SV-161	27.10.2015. 12:25:06 CEST	44.739	15.015
SV-162	27.10.2015. 12:49:13 CEST	44.742	15.021
SV-163	27.10.2015. 13:02:05 CEST	44.746	15.032
SV-164	27.10.2015. 14:05:09 CEST	44.774	15.001
SV-165	27.10.2015. 14:28:38 CEST	44.773	14.998
SV-166	27.10.2015. 14:48:12 CEST	44.773	14.997
SV-167	27.10.2015. 15:01:28 CEST	44.772	14.996
SV-168	27.10.2015. 15:36:21 CEST	44.770	14.994
SV-169	27.10.2015. 15:50:53 CEST	44.768	14.993
SV-170	27.10.2015. 16:09:25 CEST	44.767	14.990
SV-171	27.10.2015. 16:25:22 CEST	44.766	14.987
SV-172	17.7.2019 13:02:26 CEST	44.826	14.959
SV-173	17.7.2019 13:08:49 CEST	44.826	14.958
SV-174	17.7.2019 13:21:52 CEST	44.826	14.957
SV-175	17.7.2019 13:36:31 CEST	44.824	14.956
SV-176	17.7.2019 13:48:23 CEST	44.825	14.955
SV-177	17.7.2019 13:59:39 CEST	44.824	14.955
SV-178	17.7.2019 14:14:24 CEST	44.824	14.954
SV-179	17.7.2019 14:41:20 CEST	44.825	14.953
SV-180	17.7.2019 14:54:29 CEST	44.823	14.954
SV-181	17.7.2019 16:06:01 CEST	44.822	14.953
SV-182	17.7.2019 16:24:47 CEST	44.821	14.953
SV-183	17.7.2019 17:20:19 CEST	44.821	14.954
SV-184	17.7.2019 17:28:59 CEST	44.820	14.954
SV-185	17.7.2019 17:39:22 CEST	44.820	14.954
SV-186	17.7.2019 17:51:50 CEST	44.819	14.953
SV-187	17.7.2019 18:04:45 CEST	44.818	14.953
SV-188	17.7.2019 18:12:51 CEST	44.818	14.953
SV-189	18.7.2019 11:14:30 CEST	44.817	14.952
SV-190	18.7.2019 11:26:00 CEST	44.817	14.951

Location	Time created	Latitude	Longitude
SV-191	18.7.2019 11:37:07 CEST	44.817	14.950
SV-192	18.7.2019 12:01:22 CEST	44.817	14.950
SV-193	18.7.2019 12:13:13 CEST	44.817	14.949
SV-194	18.7.2019 12:33:51 CEST	44.816	14.949
SV-195	18.7.2019 12:39:00 CEST	44.816	14.948
SV-196	18.7.2019 13:05:17 CEST	44.816	14.948
SV-197	18.7.2019 13:15:45 CEST	44.816	14.947
SV-198	18.7.2019 14:10:12 CEST	44.815	14.945
SV-199	18.7.2019 14:22:25 CEST	44.815	14.945
SV-200	18.7.2019 14:34:26 CEST	44.815	14.943
SV-201	18.7.2019 14:37:19 CEST	44.816	14.943
SV-202	18.7.2019 15:48:50 CEST	44.817	14.925
SV-203	10.9.2019 15:20:39 CEST	44.816	14.942
SV-204	10.9.2019 15:33:24 CEST	44.816	14.942
SV-205	10.9.2019 15:49:47 CEST	44.816	14.941
SV-206	10.9.2019 16:05:09 CEST	44.816	14.940
SV-207	10.9.2019 16:31:55 CEST	44.817	14.940
SV-208	10.9.2019 16:41:36 CEST	44.818	14.939
SV-209	10.9.2019 17:02:12 CEST	44.818	14.937
SV-210	10.9.2019 17:31:03 CEST	44.819	14.936
SV-211	10.9.2019 17:39:40 CEST	44.818	14.935
SV-212	10.9.2019 17:52:57 CEST	44.818	14.934
SV-213	11.9.2019 13:10:56 CEST	44.819	14.933
SV-214	11.9.2019 13:23:04 CEST	44.819	14.933
SV-215	11.9.2019 13:34:26 CEST	44.820	14.933
SV-216	11.9.2019 13:43:34 CEST	44.820	14.932
SV-217	11.9.2019 13:49:45 CEST	44.820	14.932
SV-218	11.9.2019 14:01:40 CEST	44.820	14.931
SV-219	11.9.2019 14:15:38 CEST	44.820	14.930
SV-220	11.9.2019 14:27:39 CEST	44.820	14.929
SV-221	11.9.2019 14:41:25 CEST	44.819	14.928
SV-222	11.9.2019 14:45:35 CEST	44.819	14.928
SV-223	11.9.2019 14:55:37 CEST	44.819	14.927
SV-224	11.9.2019 15:36:02 CEST	44.818	14.926
SV-225	11.9.2019 15:42:37 CEST	44.817	14.925
SV-226	11.9.2019 16:03:34 CEST	44.817	14.925
SV-227	12.9.2019 11:56:27 CEST	44.816	14.925
SV-228	12.9.2019 12:05:06 CEST	44.816	14.925
SV-229	12.9.2019 12:12:33 CEST	44.816	14.924
SV-230	12.9.2019 12:22:16 CEST	44.816	14.924
SV-231	12.9.2019 12:28:55 CEST	44.816	14.924
SV-232	12.9.2019 12:33:15 CEST	44.816	14.924
SV-233	12.9.2019 12:41:46 CEST	44.815	14.924
SV-234	12.9.2019 12:45:42 CEST	44.815	14.924
SV-235	12.9.2019 12:52:14 CEST	44.815	14.924
SV-236	12.9.2019 13:01:22 CEST	44.814	14.923
SV-237	12.9.2019 13:06:36 CEST	44.814	14.923
SV-238	12.9.2019 13:36:18 CEST	44.814	14.922

Location	Time created	Latitude	Longitude
SV-239	12.9.2019 13:41:47 CEST	44.814	14.921
SV-240	12.9.2019 13:50:16 CEST	44.814	14.920
SV-241	12.9.2019 13:55:52 CEST	44.815	14.919
SV-242	12.9.2019 14:00:16 CEST	44.816	14.918
SV-243	12.9.2019 14:18:33 CEST	44.817	14.916
SV-244	12.9.2019 14:24:25 CEST	44.817	14.915
SV-245	12.9.2019 14:33:04 CEST	44.816	14.913
SV-246	12.9.2019 14:41:19 CEST	44.815	14.911
SV-247	12.9.2019 14:48:56 CEST	44.814	14.910
SV-248	19.11.2019 13:57:24 CEST	44.711	14.957
SV-249	19.11.2019 14:05:32 CEST	44.710	14.955
SV-250	19.11.2019 14:14:01 CEST	44.709	14.954
SV-251	19.11.2019 14:26:16 CEST	44.708	14.953
SV-252	19.11.2019 14:41:42 CEST	44.708	14.951
SV-253	19.11.2019 14:52:17 CEST	44.707	14.950
SV-254	19.11.2019 15:00:50 CEST	44.706	14.949
SV-255	19.11.2019 15:08:36 CEST	44.706	14.949
SV-256	19.11.2019 15:15:36 CEST	44.705	14.949
SV-257	19.11.2019 15:25:12 CEST	44.705	14.948
SV-258	19.11.2019 15:37:12 CEST	44.704	14.948
SV-259	19.11.2019 15:40:37 CEST	44.704	14.948
SV-260	19.11.2019 15:45:00 CEST	44.704	14.947
SV-261	19.11.2019 15:59:33 CEST	44.703	14.947
SV-262	19.11.2019 16:05:40 CEST	44.702	14.947
SV-263	12.10.2021 13:07:46 CEST	44.701	14.936
SV-264	12.10.2021 13:16:55 CEST	44.701	14.937
SV-265	12.10.2021 13:35:39 CEST	44.701	14.938
SV-266	12.10.2021 13:53:50 CEST	44.701	14.938
SV-267	12.10.2021 14:07:53 CEST	44.700	14.938
SV-268	12.10.2021 14:22:57 CEST	44.700	14.938
SV-269	12.10.2021 14:35:03 CEST	44.700	14.939
SV-270	12.10.2021 15:00:03 CEST	44.699	14.940
SV-271	12.10.2021 15:21:33 CEST	44.699	14.941
SV-272	12.10.2021 15:31:55 CEST	44.698	14.941
SV-273	12.10.2021 15:43:02 CEST	44.698	14.941
SV-274	12.10.2021 15:48:51 CEST	44.698	14.940
SV-275	12.10.2021 16:12:13 CEST	44.698	14.941
SV-276	12.10.2021 16:38:39 CEST	44.698	14.942
SV-277	12.10.2021 16:51:20 CEST	44.698	14.942
SV-278	12.10.2021 17:01:52 CEST	44.698	14.942
SV-279	13.10.2021 12:13:30 CEST	44.698	14.943
SV-280	13.10.2021 12:18:00 CEST	44.698	14.943
SV-281	13.10.2021 12:47:04 CEST	44.698	14.944
SV-282	13.10.2021 12:55:11 CEST	44.698	14.944
SV-283	13.10.2021 13:08:30 CEST	44.698	14.945
SV-284	13.10.2021 13:15:55 CEST	44.698	14.947
SV-285	13.10.2021 13:19:34 CEST	44.698	14.947
SV-286	13.10.2021 13:22:54 CEST	44.698	14.948

Location	Time created	Latitude	Longitude
SV-287	13.10.2021 13:28:30 CEST	44.698	14.949
SV-288	13.10.2021 13:40:03 CEST	44.699	14.949
SV-289	26.10.2021 14:46:04 CEST	44.776	14.928
SV-290	26.10.2021 14:57:58 CEST	44.776	14.928
SV-291	26.10.2021 16:06:33 CEST	44.778	14.932
SV-292	26.10.2021 16:06:38 CEST	44.776	14.928
SV-293	26.10.2021 16:31:32 CEST	44.778	14.931
SV-294	26.10.2021 16:37:26 CEST	44.778	14.931
SV-295	27.10.2021 10:47:51 CEST	44.766	14.986
SV-296	27.10.2021 10:54:11 CEST	44.766	14.986
SV-297	27.10.2021 11:03:28 CEST	44.766	14.985
SV-298	27.10.2021 11:09:32 CEST	44.766	14.984
SV-299	27.10.2021 11:13:42 CEST	44.766	14.983
SV-300	27.10.2021 11:20:36 CEST	44.766	14.982
SV-301	27.10.2021 11:30:19 CEST	44.766	14.981
SV-302	27.10.2021 11:30:29 CEST	44.766	14.981
SV-303	27.10.2021 11:39:22 CEST	44.767	14.980
SV-304	27.10.2021 11:48:10 CEST	44.767	14.980
SV-305	27.10.2021 12:03:29 CEST	44.768	14.979
SV-306	27.10.2021 12:16:01 CEST	44.769	14.978
SV-307	27.10.2021 12:24:11 CEST	44.768	14.975
SV-308	27.10.2021 12:36:20 CEST	44.768	14.975
SV-309	27.10.2021 12:44:48 CEST	44.769	14.974
SV-310	27.10.2021 12:54:32 CEST	44.768	14.972
SV-311	27.10.2021 13:07:21 CEST	44.769	14.971
SV-312	27.10.2021 13:28:27 CEST	44.769	14.969
SV-313	27.10.2021 13:33:08 CEST	44.769	14.968
SV-314	27.10.2021 13:39:15 CEST	44.769	14.967
SV-315	27.10.2021 13:45:08 CEST	44.768	14.966
SV-316	27.10.2021 13:50:17 CEST	44.768	14.965
SV-317	27.10.2021 13:58:10 CEST	44.769	14.965
SV-318	27.10.2021 14:07:25 CEST	44.769	14.964
SV-319	27.10.2021 14:13:52 CEST	44.769	14.962
SV-320	27.10.2021 14:25:05 CEST	44.770	14.961
SV-321	27.10.2021 14:31:54 CEST	44.771	14.960
SV-322	27.10.2021 14:37:00 CEST	44.771	14.960
SV-323	27.10.2021 14:48:30 CEST	44.772	14.959
SV-324	27.10.2021 14:56:39 CEST	44.772	14.959
SV-325	27.10.2021 15:09:16 CEST	44.773	14.956
SV-326	27.10.2021 15:22:08 CEST	44.773	14.954
SV-327	27.10.2021 15:30:01 CEST	44.773	14.952
SV-328	27.10.2021 15:36:43 CEST	44.773	14.952
SV-329	27.10.2021 15:53:07 CEST	44.774	14.952
SV-330	27.10.2021 15:55:30 CEST	44.775	14.951
SV-331	27.10.2021 15:59:28 CEST	44.776	14.950
SV-332	27.10.2021 16:10:51 CEST	44.777	14.947
SV-333	27.10.2021 16:17:09 CEST	44.777	14.945
SV-334	27.10.2021 16:21:12 CEST	44.778	14.944

Location	Time created	Latitude	Longitude
SV-335	27.10.2021 16:28:34 CEST	44.779	14.940
SV-336	27.10.2021 16:34:36 CEST	44.778	14.939
SV-337	27.10.2021 16:39:05 CEST	44.778	14.938
SV-338	27.10.2021 16:42:14 CEST	44.779	14.937
SV-339	28.10.2021 10:55:07 CEST	44.775	15.002
SV-340	28.10.2021 11:06:50 CEST	44.774	15.001
SV-341	28.10.2021 11:22:01 CEST	44.774	15.000
SV-342	28.10.2021 11:32:32 CEST	44.774	15.000
SV-343	28.10.2021 12:02:20 CEST	44.773	14.999
SV-344	28.10.2021 12:07:09 CEST	44.773	14.999
SV-345	28.10.2021 12:21:21 CEST	44.773	14.998
SV-346	28.10.2021 12:30:35 CEST	44.773	14.997
SV-347	28.10.2021 12:45:45 CEST	44.772	14.997
SV-348	28.10.2021 12:51:26 CEST	44.772	14.996
SV-349	28.10.2021 13:12:44 CEST	44.772	14.996
SV-350	28.10.2021 13:18:49 CEST	44.772	14.995
SV-351	28.10.2021 13:23:25 CEST	44.772	14.995
SV-352	28.10.2021 13:40:19 CEST	44.771	14.994
SV-353	28.10.2021 13:49:55 CEST	44.770	14.994
SV-354	28.10.2021 13:58:26 CEST	44.769	14.993
SV-355	28.10.2021 14:02:10 CEST	44.769	14.993
SV-356	28.10.2021 14:11:51 CEST	44.768	14.992
SV-357	28.10.2021 14:24:29 CEST	44.767	14.991
SV-358	28.10.2021 14:27:51 CEST	44.767	14.990
SV-359	28.10.2021 14:29:24 CEST	44.767	14.990
SV-360	26.10.2021 14:18:35 CEST	44.778	14.926
SV-361	26.10.2021 14:28:30 CEST	44.778	14.927
SV-362	26.10.2021 14:37:57 CEST	44.777	14.927
SV-363	26.10.2021 14:46:55 CEST	44.777	14.927
SV-364	26.10.2021 14:58:03 CEST	44.777	14.928
SV-365	26.10.2021 15:07:48 CEST	44.777	14.928
SV-366	26.10.2021 15:15:33 CEST	44.776	14.928
SV-367	26.10.2021 15:32:03 CEST	44.776	14.928
SV-368	26.10.2021 15:57:57 CEST	44.776	14.929
SV-369	26.10.2021 16:07:19 CEST	44.776	14.930
SV-370	26.10.2021 16:22:27 CEST	44.777	14.930
SV-371	26.10.2021 16:38:06 CEST	44.777	14.931
SV-372	27.10.2021 12:32:45 CEST	44.778	14.931
SV-373	27.10.2021 12:39:37 CEST	44.778	14.931
SV-374	27.10.2021 12:46:13 CEST	44.779	14.932
SV-375	27.10.2021 12:51:18 CEST	44.779	14.932
SV-376	27.10.2021 13:10:11 CEST	44.779	14.933
SV-377	27.10.2021 13:14:27 CEST	44.780	14.933
SV-378	27.10.2021 13:22:18 CEST	44.780	14.933
SV-379	27.10.2021 13:29:59 CEST	44.780	14.934
SV-380	27.10.2021 13:50:40 CEST	44.781	14.934
SV-381	27.10.2021 13:58:42 CEST	44.781	14.935
SV-382	27.10.2021 14:02:57 CEST	44.780	14.935

Location	Time created	Latitude	Longitude
SV-383	27.10.2021 14:16:53 CEST	44.780	14.935
SV-384	27.10.2021 14:31:56 CEST	44.780	14.936
SV-385	27.10.2021 14:35:11 CEST	44.780	14.936
SV-386	27.10.2021 14:38:47 CEST	44.780	14.936
SV-387	27.10.2021 14:46:14 CEST	44.779	14.937
SV-388	27.10.2021 14:55:48 CEST	44.779	14.937
SV-389	27.10.2021 15:04:58 CEST	44.779	14.937
SV-390	27.10.2021 15:53:59 CEST	44.779	14.938
SV-391	27.10.2021 15:59:58 CEST	44.778	14.938
SV-392	10.5.2022 11:44:17 CEST	44.749	15.012
SV-393	10.5.2022 11:52:44 CEST	44.751	15.011
SV-394	10.5.2022 11:58:48 CEST	44.751	15.012
SV-395	10.5.2022 12:11:40 CEST	44.753	15.012
SV-396	10.5.2022 12:44:52 CEST	44.756	15.012
SV-397	10.5.2022 12:55:53 CEST	44.757	15.013
SV-398	10.5.2022 13:09:25 CEST	44.758	15.012
SV-399	10.5.2022 13:24:39 CEST	44.761	15.010
SV-400	10.5.2022 15:00:32 CEST	44.765	15.008
SV-401	10.5.2022 15:04:05 CEST	44.765	15.008
SV-402	10.5.2022 15:10:59 CEST	44.766	15.008
SV-403	10.5.2022 15:28:36 CEST	44.767	15.009
SV-404	10.5.2022 15:40:33 CEST	44.767	15.010
SV-405	10.5.2022 16:01:48 CEST	44.768	15.010
SV-406	10.5.2022 17:50:14 CEST	44.767	15.017
SV-407	9.5.2022 13:25:10 CEST	44.854	14.927
SV-408	9.5.2022 13:53:07 CEST	44.853	14.927
SV-409	9.5.2022 14:01:20 CEST	44.853	14.927
SV-410	9.5.2022 14:12:33 CEST	44.853	14.926
SV-411	9.5.2022 14:30:10 CEST	44.852	14.926
SV-412	9.5.2022 14:38:36 CEST	44.852	14.926
SV-413	9.5.2022 14:57:08 CEST	44.852	14.925
SV-414	9.5.2022 15:10:23 CEST	44.852	14.925
SV-415	9.5.2022 15:32:01 CEST	44.851	14.924
SV-416	9.5.2022 16:17:44 CEST	44.851	14.922
SV-417	9.5.2022 16:41:42 CEST	44.849	14.921
SV-418	11.5.2022 11:19:04 CEST	44.854	14.927
SV-419	11.5.2022 11:25:34 CEST	44.854	14.928
SV-420	11.5.2022 11:34:04 CEST	44.854	14.928
SV-421	11.5.2022 12:31:40 CEST	44.853	14.929
SV-422	11.5.2022 12:52:53 CEST	44.852	14.930
SV-423	11.5.2022 13:01:45 CEST	44.852	14.931
SV-424	11.5.2022 13:19:57 CEST	44.851	14.931
SV-425	11.5.2022 13:35:47 CEST	44.850	14.934
SV-426	18.7.2022 11:49:29 CEST	44.747	15.218
SV-427	18.7.2022 13:13:37 CEST	44.731	15.261
SV-428	18.7.2022 13:52:16 CEST	44.751	15.214
SV-429	18.7.2022 14:07:42 CEST	44.751	15.215
SV-430	18.7.2022 14:50:35 CEST	44.706	15.241

Location	Time created	Latitude	Longitude
SV-431	18.7.2022 14:53:21 CEST	44.706	15.242
SV-432	18.7.2022 15:13:53 CEST	44.705	15.242
SV-433	18.7.2022 15:24:41 CEST	44.704	15.243
SV-434	18.7.2022 15:44:10 CEST	44.703	15.240
SV-435	18.7.2022 15:55:27 CEST	44.702	15.239
SV-436	18.7.2022 16:10:29 CEST	44.702	15.240
SV-437	18.7.2022 16:14:34 CEST	44.702	15.240
SV-438	18.7.2022 16:22:17 CEST	44.702	15.241
SV-439	18.7.2022 16:34:19 CEST	44.702	15.241
SV-440	18.7.2022 16:38:01 CEST	44.702	15.242
SV-441	18.7.2022 16:43:29 CEST	44.703	15.243
SV-442	18.7.2022 16:56:14 CEST	44.702	15.245
SV-443	19.7.2022 10:21:34 CEST	44.712	15.183
SV-444	19.7.2022 10:52:02 CEST	44.712	15.184
SV-445	19.7.2022 11:05:07 CEST	44.711	15.186
SV-446	19.7.2022 11:17:52 CEST	44.708	15.166
SV-447	19.7.2022 11:34:08 CEST	44.710	15.139
SV-448	19.7.2022 11:51:36 CEST	44.710	15.137
SV-449	19.7.2022 12:20:41 CEST	44.714	15.121
SV-450	19.7.2022 12:29:31 CEST	44.715	15.119
SV-451	19.7.2022 12:51:19 CEST	44.716	15.113
SV-452	19.7.2022 12:54:48 CEST	44.715	15.111
SV-453	19.7.2022 13:00:12 CEST	44.715	15.111
SV-454	19.7.2022 13:55:24 CEST	44.717	15.100
SV-455	19.7.2022 14:16:37 CEST	44.719	15.075
SV-456	19.7.2022 14:40:20 CEST	44.720	15.055
SV-457	19.7.2022 14:45:47 CEST	44.721	15.055
SV-458	19.7.2022 14:55:41 CEST	44.721	15.055
SV-459	19.7.2022 15:10:45 CEST	44.718	15.056
SV-460	19.7.2022 16:23:10 CEST	44.738	15.101
SV-461	19.7.2022 16:35:03 CEST	44.734	15.113
SV-462	19.7.2022 16:39:58 CEST	44.733	15.122
SV-463	19.7.2022 16:51:05 CEST	44.728	15.131
SV-464	19.7.2022 16:59:51 CEST	44.720	15.143
SV-465	19.7.2022 17:11:48 CEST	44.718	15.154
SV-466	19.7.2022 17:21:15 CEST	44.713	15.161
SV-467	20.7.2022 10:48:03 CEST	44.777	15.002
SV-468	20.7.2022 10:55:38 CEST	44.779	15.002
SV-469	20.7.2022 11:03:30 CEST	44.779	15.002
SV-470	20.7.2022 11:11:35 CEST	44.781	15.003
SV-471	20.7.2022 11:15:31 CEST	44.781	15.004
SV-472	20.7.2022 11:24:15 CEST	44.782	15.005
SV-473	20.7.2022 11:32:47 CEST	44.783	15.006
SV-474	20.7.2022 11:45:50 CEST	44.784	15.007
SV-475	20.7.2022 12:03:17 CEST	44.784	15.009
SV-476	20.7.2022 12:22:31 CEST	44.786	15.008
SV-477	20.7.2022 12:29:57 CEST	44.786	15.007
SV-478	20.7.2022 13:35:08 CEST	44.739	15.101

Location	Time created	Latitude	Longitude
SV-479	20.7.2022 13:45:21 CEST	44.740	15.099
SV-480	20.7.2022 13:54:08 CEST	44.742	15.098
SV-481	20.7.2022 14:04:03 CEST	44.744	15.095
SV-482	20.7.2022 14:12:11 CEST	44.747	15.094
SV-483	20.7.2022 14:24:54 CEST	44.749	15.097
SV-484	25.9.2022 9:51:30 CEST	44.803	14.983
SV-485	25.9.2022 10:00:53 CEST	44.799	14.984
SV-486	25.9.2022 10:16:29 CEST	44.794	14.984
SV-487	25.9.2022 10:20:12 CEST	44.794	14.984
SV-488	25.9.2022 10:25:38 CEST	44.793	14.984
SV-489	25.9.2022 10:44:51 CEST	44.792	14.985
SV-490	25.9.2022 10:51:16 CEST	44.792	14.985
SV-491	25.9.2022 10:57:54 CEST	44.791	14.985
SV-492	25.9.2022 11:12:19 CEST	44.790	14.985
SV-493	25.9.2022 11:26:22 CEST	44.789	14.986
SV-494	25.9.2022 11:39:57 CEST	44.789	14.986
SV-495	25.9.2022 11:45:44 CEST	44.789	14.986
SV-496	25.9.2022 11:56:24 CEST	44.789	14.986
SV-497	25.9.2022 12:04:22 CEST	44.788	14.987
SV-498	25.9.2022 12:10:44 CEST	44.788	14.987
SV-499	25.9.2022 12:16:29 CEST	44.787	14.987
SV-500	25.9.2022 12:23:31 CEST	44.787	14.987
SV-501	25.9.2022 12:32:41 CEST	44.787	14.987
SV-502	25.9.2022 12:45:13 CEST	44.787	14.987
SV-503	25.9.2022 13:00:25 CEST	44.786	14.987
SV-504	25.9.2022 15:15:45 CEST	44.766	14.987
SV-505	25.9.2022 15:22:45 CEST	44.766	14.988
SV-506	25.9.2022 15:34:56 CEST	44.766	14.989

Location	Time created	Latitude	Longitude
SV-507	25.9.2022 15:40:21 CEST	44.767	14.989
SV-508	25.9.2022 15:48:58 CEST	44.767	14.990
SV-509	25.9.2022 15:54:03 CEST	44.768	14.989
SV-510	25.9.2022 15:57:59 CEST	44.769	14.989
SV-511	25.9.2022 16:03:42 CEST	44.769	14.989
SV-512	25.9.2022 16:14:12 CEST	44.770	14.989
SV-513	25.9.2022 16:23:18 CEST	44.770	14.988
SV-514	25.9.2022 16:29:30 CEST	44.770	14.988
SV-515	25.9.2022 16:35:16 CEST	44.771	14.988
SV-516	25.9.2022 16:42:59 CEST	44.771	14.987
SV-517	25.9.2022 16:49:07 CEST	44.772	14.988
SV-518	25.9.2022 16:52:56 CEST	44.772	14.988
SV-519	25.9.2022 16:55:54 CEST	44.772	14.988
SV-520	25.9.2022 16:59:42 CEST	44.772	14.988
SV-521	25.9.2022 17:07:40 CEST	44.773	14.988
SV-522	25.9.2022 17:16:07 CEST	44.773	14.987
SV-523	25.9.2022 17:26:31 CEST	44.774	14.986
SV-524	25.9.2022 17:31:08 CEST	44.774	14.986
SV-525	25.9.2022 17:40:06 CEST	44.775	14.985
SV-526	25.9.2022 17:49:15 CEST	44.775	14.985
SV-527	25.9.2022 17:53:42 CEST	44.776	14.985
SV-528	25.9.2022 17:59:40 CEST	44.776	14.985
SV-529	25.9.2022 18:06:02 CEST	44.776	14.985
SV-530	25.9.2022 18:10:01 CEST	44.777	14.985
SV-531	25.9.2022 18:15:20 CEST	44.777	14.984
SV-532	25.9.2022 18:17:10 CEST	44.777	14.984
SV-533	25.9.2022 18:24:29 CEST	44.778	14.983

Supplement 2. Profiles – sampling locations

Field profile	Profile name	Start location		End location		Total length	Sample	Sample location	
		Latitude (°N)	Longitude (°E)	Latitude (°N)	Longitude (°E)	(km)		Latitude (°N)	Longitude (°E)
P1	Trnovac – Rogić dolina	44,847	14,920	44,850	14,934	1.65	SV-22-R-1	44.854	14.927
							SV-22-R-10	44.851	14.922
							SV-22-R-14	44.854	14.928
							SV-22-R-15	44.853	14.929
							SV-22-R-16	44.852	14.930
							SV-22-R-5	44.852	14.926
							SV-22-R-6	44.852	14.926
							SV-22-R-8	44.852	14.925
							SV-22-R-9	44.851	14.924
P2	Babic Sica – Gornja Klada	44,814	14,909	44,839	14,966	7.12	SV-30	44.817	14.925
							SV-36	44.818	14.939
							SV-37	44.818	14.937
							SV-42	44.819	14.933
							SV-58a	44.816	14.924
							SV-58b	44.816	14.924
							SV-66	44.814	14.920
							SV-69	44.817	14.916
							SV-70	44.817	14.915
							SV-12	44.820	14.954
							SV-15A	44.818	14.953
							SV-15B	44.818	14.953
							SV-16	44.818	14.953
							SV-19	44.817	14.950
							SV-2	44.826	14.958
							SV-20	44.817	14.950
							SV-21	44.817	14.949
							SV-23	44.816	14.948
							SV-2A	44.826	14.957
							SV-4	44.825	14.955
							SV-6	44.824	14.954
							SV-8	44.823	14.954
							SV-9	44.822	14.953
P3	Velike Brisnice – Livadica	44,778	14,926	44,786	15,007	13.12	SV-04-22	44.777	14.927
							SV-08-22	44.776	14.928
							SV-11-22	44.777	14.930
							SV-113-21	44.767	14.980
							SV-120-21	44.769	14.971
							SV-133-21	44.772	14.959
							SV-134-21	44.773	14.956
							SV-18-22	44.780	14.933
							SV-21-29	44.778	14.932
							SV-29-22	44.779	14.937

Field profile	Profile name	Start location		End location		Total length	Sample	Sample location	
		Latitude (°N)	Longitude (°E)	Latitude (°N)	Longitude (°E)	(km)		Latitude (°N)	Longitude (°E)
P4	Zavižan – Rossijeva koliba	44,803	14,982	44,767	14,990	3.91	–	–	–
P5	Veliki Lubenovac – Hajdučki Kukovi	44,748	15,011	44,767	15,017	2.96	–	–	–
P6	Jablanac – Alan	44,701	14,936	44,710	14,956	3.86	SV-80	44.706	14.949
							SV-21-02	44.701	14.937
							SV-21-04	44.701	14.938
							SV-21-13	44.698	14.940
							SV-21-15	44.698	14.942
							SV-21-19	44.698	14.943
							SV-21-21	44.698	14.944
							SV-21-26	44.698	14.949
							SV-21-27	44.699	14.949
							SV-21-3	44.701	14.938
							SV-21-8	44.699	14.940
P7	Kosinj – Vranjkova draga	44,710	15,187	44,717	15,056	11.47	–	–	–
P8	Kosinjski Bakovac – Mračaj	44,707	15,244	44,749	15,096	14.58	–	–	–